AGU PUBLICATIONS

JGR

Journal of Geophysical Research: Oceans

RESEARCH ARTICLE

10.1002/2016JC011634

Studies of the Canadian Arctic Archipelago water transport and its relationship to basin-local forcings: Results from AO-FVCOM

Yu Zhang[1,2], Changsheng Chen[1,2], Robert C. Beardsley[3], Guoping Gao[2], Zhigang Lai[4], Beth Curry[5], Craig M. Lee[5], Huichan Lin[1], Jianhua Qi[1], and Qichun Xu[1]

[1]School for Marine Science and Technology, University of Massachusetts-Dartmouth, New Bedford, Massachusetts, USA, [2]International Center for Marine Studies, Shanghai Ocean University, Shanghai, China, [3]Department of Physical Oceanography, Woods Hole Oceanographic Institution, Woods Hole, Massachusetts, USA, [4]School of Marine Sciences, Sun Yat-Sen University, Guangzhou, China, [5]Applied Physics Laboratory, University of Washington, Seattle, Washington, USA

Key Points:
- A high-resolution Arctic Ocean FVCOM is capable of simulating the CAA outflow
- The basin-scale sea level pressure is a major driver of the CAA outflow
- The volume flux through Davis Strait is negatively correlated with the flux through Fram Strait

Correspondence to:
Y. Zhang,
yzhang3@umassd.edu

Citation:
Zhang, Y., C. Chen, R. C. Beardsley, G. Gao, Z. Lai, B. Curry, C. M. Lee, H. Lin, J. Qi, and Q. Xu (2016), Studies of the Canadian Arctic Archipelago water transport and its relationship to basin-local forcings: Results from AO-FVCOM, *J. Geophys. Res. Oceans*, *121*, 4392–4415, doi:10.1002/2016JC011634.

Received 8 JAN 2016
Accepted 27 MAY 2016
Accepted article online 2 JUN 2016
Published online 25 JUN 2016

Abstract A high-resolution (up to 2 km), unstructured-grid, fully coupled Arctic sea ice-ocean Finite-Volume Community Ocean Model (AO-FVCOM) was employed to simulate the flow and transport through the Canadian Arctic Archipelago (CAA) over the period 1978–2013. The model-simulated CAA outflow flux was in reasonable agreement with the flux estimated based on measurements across Davis Strait, Nares Strait, Lancaster Sound, and Jones Sounds. The model was capable of reproducing the observed interannual variability in Davis Strait and Lancaster Sound. The simulated CAA outflow transport was highly correlated with the along-strait and cross-strait sea surface height (SSH) difference. Compared with the wind forcing, the sea level pressure (SLP) played a dominant role in establishing the SSH difference and the correlation of the CAA outflow with the cross-strait SSH difference can be explained by a simple geostrophic balance. The change in the simulated CAA outflow transport through Davis Strait showed a negative correlation with the net flux through Fram Strait. This correlation was related to the variation of the spatial distribution and intensity of the slope current over the Beaufort Sea and Greenland shelves. The different basin-scale surface forcings can increase the model uncertainty in the CAA outflow flux up to 15%. The daily adjustment of the model elevation to the satellite-derived SSH in the North Atlantic region outside Fram Strait could produce a larger North Atlantic inflow through west Svalbard and weaken the outflow from the Arctic Ocean through east Greenland.

1. Introduction

The Arctic Ocean is a polar basin with its major water sources consisting of relatively cold and fresh Pacific water inflowing through Bering Strait [*Coachman and Aagaard*, 1988], relatively warm and salty Atlantic water entering through Fram Strait and the Barents Sea [*Fahrbach et al.*, 2001] and river runoff (Figure 1). These water inflows coexist with outflows through two pathways: the Canadian Arctic Archipelago (CAA) Straits and the eastern shelf of Greenland connected to Fram Strait [*Aagaard and Carmack*, 1989]. The CAA is characterized by numerous islands, straits, and narrow and shallow channels or water passages. The CAA water from Nares Strait, Lancaster Sound, and Jones Sound flows into Baffin Bay and then enters the North Atlantic Ocean through Davis Strait [*Tang et al.*, 2004; *Cuny et al.*, 2005; *Curry et al.*, 2011, 2014], with a small portion flowing into the Labrador Sea through Hudson Strait [*Straneo and Saucier*, 2008]. Fram Strait can carry the warm and salty Atlantic inflow named the West Spitsbergen Current (WSC) along the western coast of Spitsbergen and the cold and fresh Arctic outflow named the East Greenland Current (EGC) [*Schlichtholz and Houssais*, 1999; *Woodgate et al.*, 1999].

The inflow and outflow transports through the Arctic varied seasonally and interannually in responses to the basin-scale forcing with influences of global climate change [e.g., *Jahn et al.*, 2010; *McGeehan and Maslowski*, 2012; *Wekerle et al.*, 2013]. The qualitative and accurate estimation of these variabilities, in turn, is critical to understanding the changes in the Arctic and the impacts on the North Atlantic Ocean. In the past decades, many measurements have been made to estimate the transports through Bering Strait [*Coachman and Aagaard*, 1988; *Roach et al.*, 1995; *Woodgate et al.*, 2005, 2006, 2010] and Fram Strait [*Fahrbach et al.*, 2001; *Schauer et al.*, 2004, 2008; *Rudels et al.*, 2008], but only a few were made in the Barents Sea Opening [*Ingvaldsen et al.*, 2004; *Skagseth et al.*, 2008] and the CAA. The measurements in the CAA were mainly

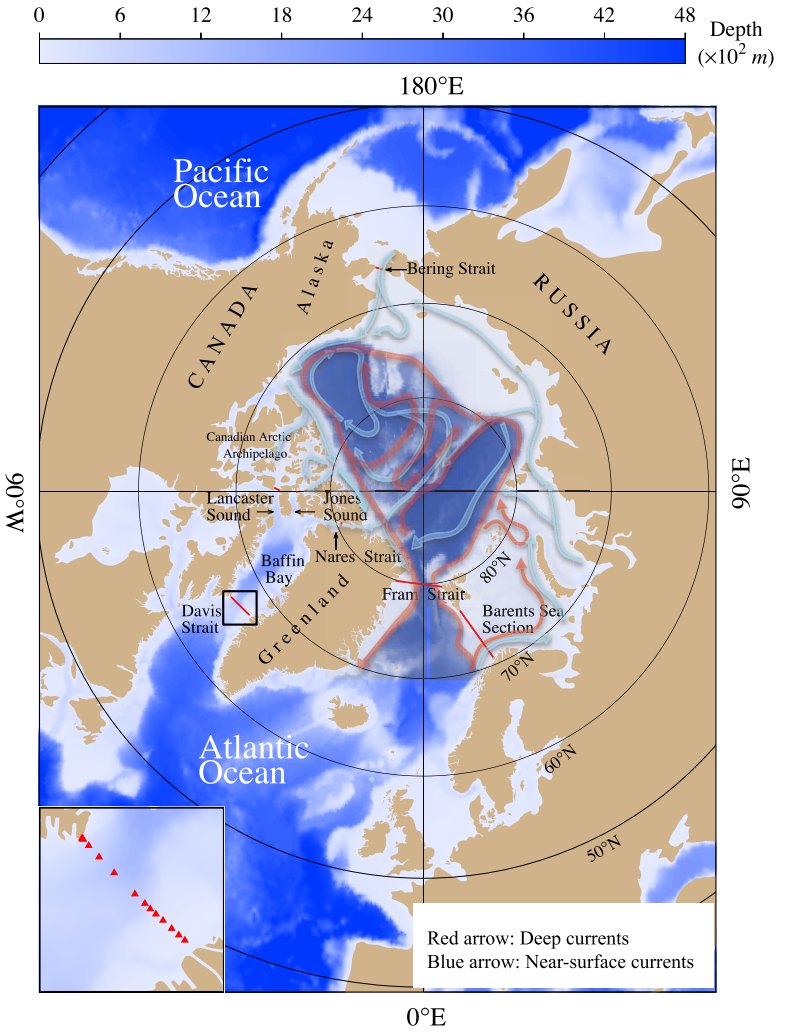

Figure 1. Bathymetry and schematic of near-surface and deep circulations in the Arctic Ocean. Red arrows: the deep currents. Blue arrows: the near-surface currents. Red lines: the sections where the volume flux was estimated. Box: the area of Davis Strait that is displayed enlarged in the lower-left corner. The red triangles indicate the locations of current/hydrographic measurement sites in Davis Strait.

focused on Nares Strait [*Sadler*, 1976; *Münchow et al*., 2006, 2007; *Münchow and Melling*, 2008], Lancaster Sound [*Prinsenberg and Hamilton*, 2005; *Melling et al*., 2008; *Prinsenberg et al*., 2009; *Peterson et al*., 2012], and Jones Sound [*Melling et al*., 2008], as well as Davis Strait-a downstream strait capturing water transports from the three main water pathways [*Cuny et al*., 2005; *Curry et al*., 2011, 2014].

Our current understanding on the variability of the CAA outflow is mainly based on both observational findings and basin-scale Arctic Ocean models. Previous observations suggested that the sea surface height (SSH) difference between the Arctic shelf and Baffin Bay is the key mechanism to control the CAA outflow transport [e.g., *Münchow and Melling*, 2008; *Peterson et al*., 2012]. Several modeling efforts were made to examine physical processes controlling the SSH variation in the CAA. Due to differences in discrete algorithm, grid resolution, bathymetry and coastline approximation, external driving forcing and lateral boundary conditions, etc., however, the findings obtained from these models were diverse, often not consistent, and the mechanisms produced by them differed substantially in terms of particulars [*Jahn et al*., 2010; *Houssais and Herbaut*, 2011; *McGeehan and Maslowski*, 2012; *Wekerle et al*., 2013; *Lu et al*., 2014]. What are key external forcing components, winds or sea level pressure (SLP) or both, attributing to the onset and variability of the SSH difference and thus the CAA outflow? To our knowledge, this question has not been well understood yet in term of a quantitative assessment.

It is well known that Fram Strait and the CAA are the two regions for the Arctic Ocean water outflows. The outflow along the east Greenland coast of Fram Strait consists of two major current pathways: one is from

the cyclonic circulation in the Eurasian Basin and along the Lomonosov Ridge and the other is the cyclonic slope currents from the Beaufort Sea/Canadian Basin (Figure 1). Assuming that the inflow and outflow are balanced, when the inflows are given, the variation of the outflow through the CAA could affect the net flux through Fram Strait. This suggests that a state-of-the-art Arctic Ocean model should have a sufficient resolution to be capable of resolving both basin and local-scale physical processes, particularly with better representing the complex geometry of the CAA including narrow straits and water passages. This type of multiscale resolving model could provide us a tool to examine the role of the CAA in the Arctic Ocean system.

The upper ocean circulation in the Arctic is dominated by the wind-drifting-driven and ice-drifting-driven anticyclonic circulation [*Proshutinsky et al*., 2001; *Steele et al*., 2001; *Holloway et al*., 2007; *Chen et al*., 2016]. Due to its severe natural conditions and limitations in past research efforts, the Arctic still remains in an insufficient monitoring status for both meteorological and oceanic conditions [*Wekerle et al*., 2013]. The external forcing used to force a model is based fully on the regional or global meteorological model outputs with the lack of validation or calibration through observations. What level could a model-produced CAA outflow transport be affected when different meteorological forcings are used? Is it critical to resolve the local wind variability in narrow straits of the CAA when the CAA outflow is simulated? These questions should be addressed, since a fair model-data comparison is required to take the model uncertainty into account.

Fram Strait is an inflow-outflow strait containing both the North Atlantic inflow along the west coast of Svalbard and the Arctic outflow along the east Greenland shelf. Whether or not a model can well produce the North Atlantic inflow directly affects the reality and accuracy of the net outflow flux through Fram Strait and hence the circulation and ice in the Arctic basin. When a regional model is applied to the Arctic Ocean, one is required to set up the boundary conditions in both Atlantic and Pacific Ocean. Either one-way or two-way nesting with a global model is a common approach used in the Arctic Ocean model simulation. As long as Fram Strait is considered, the success of this approach depends on whether or not a global model could provide an accurate simulation of the North Atlantic water flux on the nesting boundary. The satellite-derived SSH is widely used in the global ocean models to improve the low-frequency spatial variation of the gradient of the sea surface elevation and thus the barotropic component of the ocean circulation [*Marshall et al*., 1997; *Madec et al*., 1998; *Pacanowsky and Griffies*, 1999; *Smith and Gent*, 2002; *Bleck et al*., 2002; *Chassignet et al*., 2003, 2006; *Chen et al*., 2016]. The Archiving, Validation, and Interpretation of Satellite Oceanographic data (AVISO) daily satellite-derived SSH product covers the ocean region bounded by ~80°S–80°N. How will a regional Arctic Ocean model perform with the data assimilation of the satellite-derived SSH in the Arctic Ocean? How will the net flux through Fram Strait change when the SSH assimilation is taken into account? Conducting the model experiments with and without the SSH assimilation could help us not only address these questions but also explore the dynamics controlling the net flux through Fram Strait.

A new high-resolution, global-basin nested, ice-sea coupled Arctic Ocean model was developed based on the unstructured-grid, Finite-Volume Community Ocean Model (hereafter referred to as AO-FVCOM) [*Chen et al*., 2009; *Gao et al*., 2011; *Chen et al*., 2016]. The model was designed to meet the following state-of-the-art Arctic Ocean model requirements: (a) grid flexibility to resolve the complex coastal geometry and steep continental slopes; (b) mass conservation in a numerical computational sense to accurately simulate mass, heat, and salt transport; (c) proper parameterization of vertical and lateral mixing to capture water stratification; (d) advanced data assimilation methods to integrate observations with simulation results; and (e) modular structures to facilitate process-oriented and hindcast/forecast applications [*Chen et al*., 2013]. Using the AO-FVCOM, we have simulated the sea ice and circulation in the Arctic for the period 1978–2013. The AO-FVCOM simulation results provide us with an opportunity to validate this model through comparisons with observations in the CAA and examine the physical processes controlling Arctic outflow through the CAA.

In this paper, we attempt to address the questions described above. The simulated water transport is first compared with observations taken in the CAA and Davis Strait to ensure the ability of the AO-FVCOM to reasonably capture the seasonal and interannual variability of the CAA outflow. Then a series of process-oriented model-experiments are conducted to examine the local and basin-scale physical processes associated with external forcing.

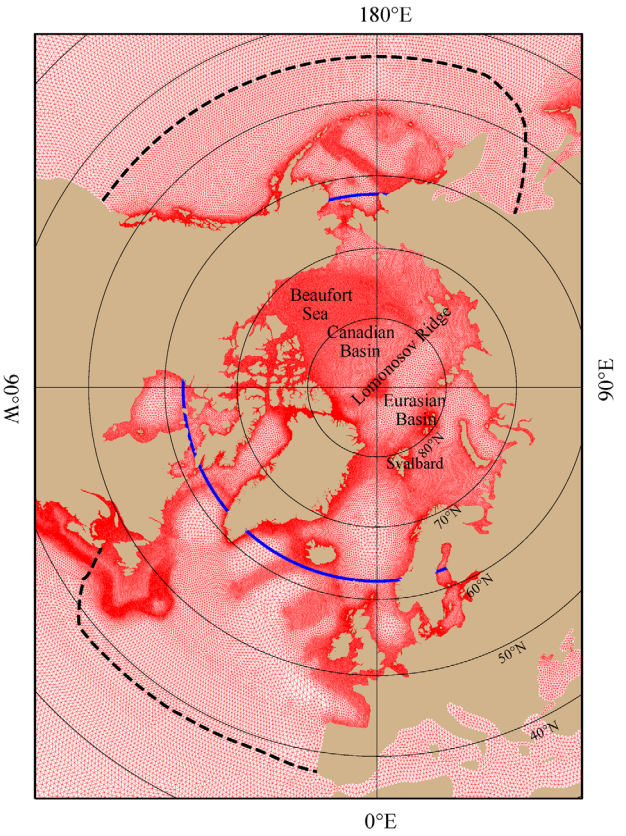

Figure 2. The unstructured triangular gird of the AO-FVCOM nested with Global-FVCOM. Black dash lines indicate the nesting boundaries of AO-FVCOM and Global-FVCOM. Blue line indicates the 62.5°N line, the northern boundary of SST and SSH assimilation. For the 36 year simulation, the AO-FVCOM was run by merging it to the Global-FVCOM with a horizontal resolution up to 2 km in the Canadian Arctic Archipelago.

The rest of the paper is organized as follows. In section 2, the model setup and observational data are briefly described. In section 3, the comparison of observed and simulated water transports through the CAA and Davis Strait is presented. In section 4, the process-oriented experiment results are discussed, with a focus on the response of the CAA outflow to the local and basin-scale variability. In section 5, sensitivities of the model performance to external forcing, grid refinement and SSH assimilation are examined. Conclusions are summarized following discussions in section 6.

2. AO-FVCOM and Observational Data

2.1. AO-FVCOM

The AO-FVCOM is an Arctic regional coupled ice-ocean model nested within the global FVCOM modeling system [*Chen et al.*, 2016]. The FVCOM is a prognostic, unstructured-grid, Finite-Volume, free-surface, 3-D primitive equation Community Ocean Model [*Chen et al.*, 2003, 2006, 2007, 2013]. The AO-FVCOM is configured using a spherical coordinate version of FVCOM with a horizontal resolution varying from 2 to 40 km, with a mean resolution of ~5 km in the CAA and ~12 km in the central Arctic Ocean (Figure 2). A hybrid terrain-following coordinate is used in the vertical, with a total of 45 layers. The *s*-coordinate is used in the region deeper than and equal 225 m, with 10 uniform layers (thickness of 5 m) near the surface and five uniform layers (thickness of 5 m) near the bottom, respectively. The σ-coordinate is specified in the shallow continental and coastal regions of less than 225 m. These s-coordinate and σ-coordinate have a transition at the 225-isobath at which the thickness of all layers is 5 m. The AO-FVCOM can run either through nesting with Global-FVCOM or by merging into Global-FVCOM as a single global-scale model. Global-FVCOM has a horizontal resolution of up to 2 km and the same vertical resolution as AO-FVCOM. The ice model coupled in AO-FVCOM and Global-FVCOM is UG-CICE: an unstructured-grid, finite-volume version of the Los Alamos Community Ice Code developed by *Gao et al.* [2011].

The 36 year (1978–2013) simulation was conducted by Global-FVCOM merging with AO-FVCOM with resolution up to 2 km. The model was initialized with the 50 year spin-up output under a "climatologic" meteorological forcing and river discharge conditions [*Gao et al.*, 2011] and driven by (a) astronomical tidal forcing with eight constituents (M_2, S_2, N_2, K_2, K_1, P_1, O_1, and Q_1), (b) surface wind stress, (c) net heat flux at the surface plus shortwave irradiance in the water column, (d) surface air pressure gradients, (e) precipitation (P) minus evaporation (E), and (f) river discharges [*Gao et al.*, 2011; *Chen et al.*, 2016].

The 1978–2013 simulation began on 1 January 1978. The atmospheric forcing was taken from the 6 hourly version-2 data set for the Common Ocean-ice Reference Experiments (CORE-v2) over the period 1978–2009 and then the National Center for Environmental Prediction and the National Center for Atmospheric Research (NCEP/NCAR) data set over the period 2010–2013. A total of 766 rivers were included in the Global-FVCOM. The river discharges collected from the U.S. Geological Survey and the Water Survey of

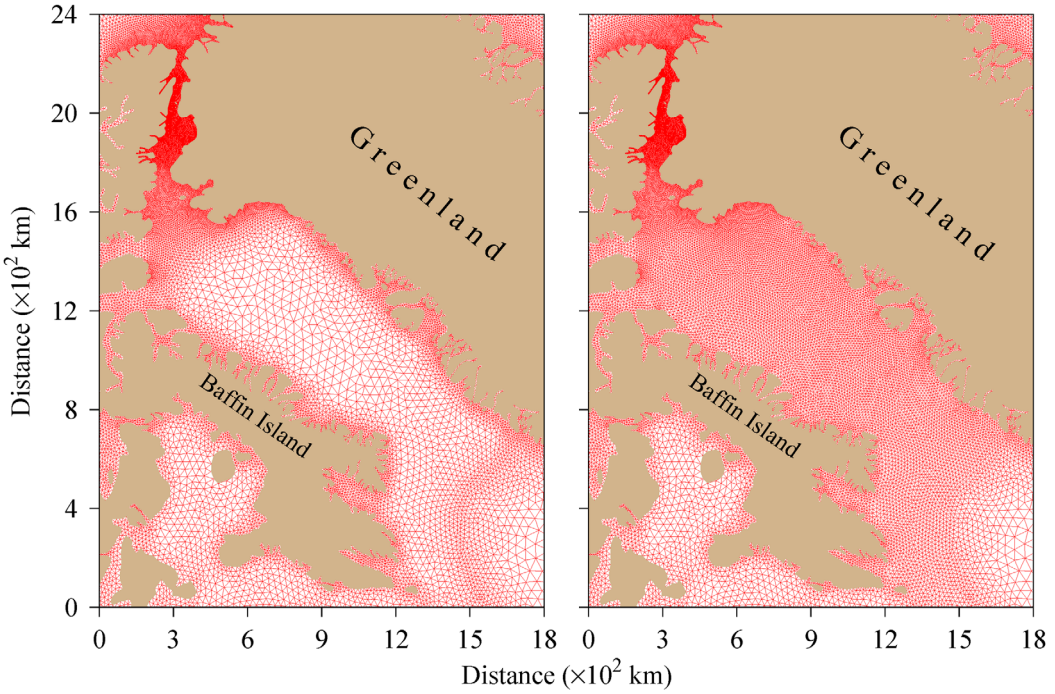

Figure 3. (left) Original and (right) refined unstructured triangular grids configured in the Baffin Bay region used in the sensitivity experiments. The horizontal resolutions were 35 and 8 km in this region, respectively, for the cases with original and refined AO-FVCOM grids.

Canada were specified using daily real-time records. For the rivers without real-time discharge records, the climatologically averaged daily records were used. To adjust the initial climatologic temperature and salinity to the real-time observation, the satellite-derived global daily sea surface temperature (SST) (ftp://data.nodc.noaa.gov/pub/data.nodc/ghrsst/) and sea surface height (SSH) (http://www.aviso.altimetry.fr/en/data/products/sea-surface-height-products/global/msla-h.html) south of 62.5°N was assimilated into Global-FVCOM by a nudging method. Given a priori statistical assumption about the model noise and errors in the observational data, this assimilation method was to merge model-predicted values directly to observations [*Chen et al*., 2013]. The SST assimilation was conducted through the surface mixed layer with its thickness (which could be tens of meters) being determined using the PWP mixed layer model [*Price et al*., 1986]. We collected all available T/S observational data (e.g., NODC, JAMSTEC, and Argo) and assimilated this into the Global-FVCOM on the monthly averaged scale to help ensure simulated stratification would be consistent with observations. The model used a modified Mellor and Yamada level 2.5 (MY-2.5) and Smagorinsky turbulent closure schemes for vertical and horizontal mixing, respectively [*Mellor and Yamada*, 1982; *Galperin et al*., 1988; *Smagorinsky*, 1963]. The time step used for integration was 300 s.

To examine the sensitivity of the simulated CAA outflow to external forcing, we reran the simulation with different atmospheric forcing from the NCEP/NCAR reanalysis and the European Centre for Medium-Range Weather Forecasts (ECMWF) data sets as well as in addition the high-resolution (∼6 km) hourly polar wind field produced by the Fifth-Generation Penn State/NCAR Mesoscale Model (MM5) for the period 2004–2010. To evaluate the influence of model resolution on the accuracy of the simulated CAA outflow, we also reran the model by refining the grid from 35 to 8 km in Baffin Bay (Figure 3).

2.2. Observational Data

The simulated CAA outflow transport was compared with the observations of currents across Davis Strait (Figure 1). The Bedford Institute of Oceanography (BIO) deployed six moorings across Davis Strait in September 1987 and the records covered the period until August 1990 [*Cuny et al*., 2005]. The separation distance between moorings was about 30–60 km. At each mooring, three Aanderaa Recording Current Meters (RCM5) were mounted at depths of around 150, 300, and 500 m. A new set of moorings were deployed again in September 2004, with 14 moorings: 4 on the shelf of Baffin Island, 4 on the shelf of western Greenland, and 6 in the interior of the strait [*Curry et al*., 2011]. The number of moorings varied with the years.

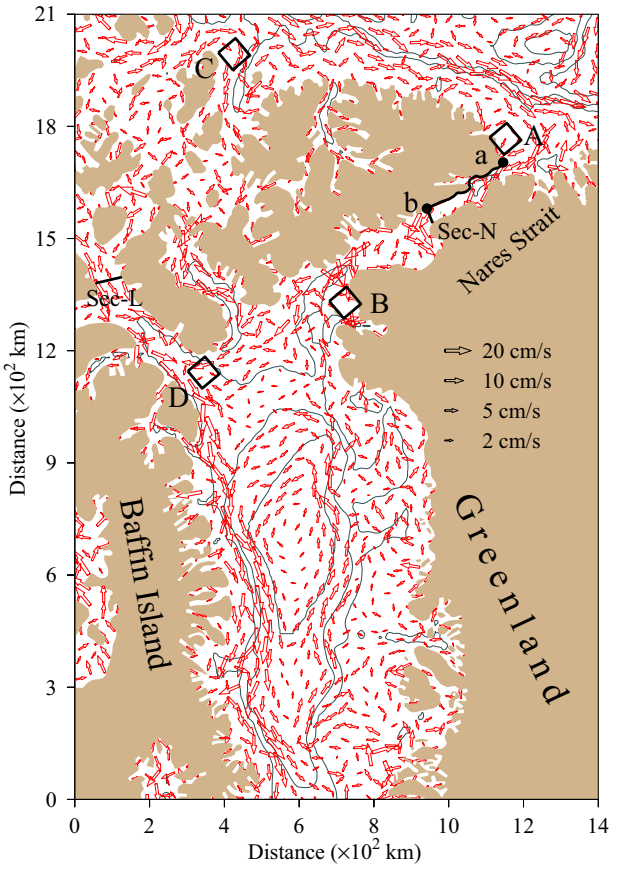

Figure 4. The distribution of the mean current vectors averaged in the upper 400 m and over a 36 year period of 1978–2013 in Baffin Bay with connection to Nares Strait, Lancaster Sound, and Jones Sound. The currents were rescaled using the root-square vector scale and resampled with a 35 km resolution to make vectors visible. Black boxes: the area where the mean simulated SSH was calculated in the upstream and downstream of Nares Strait and Lancaster Sound. Black lines: the sections where the SSH difference was calculated in Nares Strait and Lancaster Sound. The back line connected between *a* and *b* is the streamline used for the analytical solution.

During the year 2009–2010, it became 12 moorings: 2 on the shelf of Baffin Island, 4 on the shelf of the western Greenland, and 6 in the interior of the strait [*Curry et al.*, 2014]. The separation distance of these moorings varied from ~0.1 to 26 km over the shelf to ~16–65 km in the interior. Acoustic Doppler Current Profilers (ADCP) were mounted in the depth between 56 and 390 m and Sea-Bird Electronics (SBE) 37 MicroCATs were mounted in the depth between 20 and 500 m depending on the location [*Curry et al.*, 2014]. At each mooring in the interior of the strait, 1-3 Aanderaa Recording Current Meters (RCM8) were mounted in the deep region between 200 and 500 m. A detailed summary of the locations, depths, record lengths, and types of instruments deployed between September 2004 and September 2010 was published in the appendix of *Curry et al.* [2014]. We also compared the model results with observations taken in Nares Strait [*Sadler*, 1976; *Münchow et al.*, 2006, 2007; *Münchow and Melling*, 2008], Lancaster Sound [*Peterson et al.*, 2012; *Prinsenberg and Hamilton*, 2005; *Melling et al.*, 2008; *Prinsenberg et al.*, 2009; *Peterson et al.*, 2012], and Jones Sound [*Melling et al.*, 2008]. To examine the dynamical relationship of the CAA outflow transport with the Arctic Basin variability, the simulated transports were compared with the observations taken in Bering Strait [*Coachman and Aagaard*, 1988; *Roach et al.*, 1995; *Woodgate et al.*, 2005, 2006, 2010], Barents Sea Opening [*Ingvaldsen et al.*, 2004; *Skagseth et al.*, 2008], and Fram Strait [*Fahrbach et al.*, 2001; *Schauer et al.*, 2004, 2008; *Rudels et al.*, 2008] .

3. Validations of the Simulated CAA Water Transport

3.1. Mean Transport

The CAA outflows from Nares Strait, Lancaster Sound, and Jones Sound enter the North Atlantic Ocean through Davis Strait. The geometries of major water passages of the CAA were reasonably resolved in AO-FVCOM and the simulated 36 year averaged results captured the CAA circulation pattern suggested by previous observations. The AO-FVCOM showed the coastal-intensified outflows through Nares Strait, Lancaster Sound and Johnes Sound (Figure 4). These flows brought the relarively cold and fresher water into Davis Strait to form a strong southward coastal current named the "Baffin Island Current (BIC)" along the western shelf of Davis Strait [*Tang et al.*, 2004; *Cuny et al.*, 2005]. The model suggested a flow connectivity among these three CAA outflow passages, which directly contributed to the formation of BIC. Davis Strait was characterized by the northward inflow along the eastern slope and shelf, which could be traced back to the inflow of mixed West Greenland Coastal and Slope Currents like the observations described in *Curry et al.* [2014].

Table 1. Comparison of the Volume Flux Between AO-FVCOM and Observational Estimates[a]

	FVCOM (Sv)			
Location	Vol. Flux	Std.	Obs. (Sv)	Source
Davis Strait	−1.83	0.80		Simulation (1978–2013)
	−1.51	0.46	−2.6 ± 1.0	*Cuny et al.* [2005] (Sep 1987 to Aug 1990)
	−1.94	0.61	−2.3 ± 0.7	*Curry et al.* [2011] (Oct 2004 to Sep 2005)
	−2.14	0.76	−1.6 ± 0.2	*Curry et al.* [2014] (Oct 2004 to Sep 2010)
Nares Strait	−0.81	0.33		Simulation (1978–2013)
			−0.67 ± 0.1	*Sadler* [1976] (Apr to Jun 1972)
	−0.73	0.48	−0.8 ± 0.3	*Münchow et al.* [2006] (Aug 2003)
	−0.73	0.48	−0.91 ± 0.1	*Münchow et al.* [2007] (Aug 2003)
	−0.85	0.32	−0.57 ± 0.09	*Münchow and Melling* [2008] (Aug 2003 to Aug 2006)
Lancaster Sound	−0.71	0.17		Simulation (1978–2013)
	−0.70	0.30	−0.75 ± 0.25	*Prinsenberg and Hamilton* [2005] (Aug 1998 to Sep 2001)
				Melling et al. [2008] (Aug 1998 to Aug 2004)
	−0.68	0.32	−0.7 ± 0.4	*Prinsenberg et al.* [2009] (Aug 1998 to Aug 2006)
	−0.65	0.32	−0.7 ± 0.3	*Peterson et al.* [2012] (Aug 1998 to Aug 2006)
	−0.65	0.32	−0.53	*Peterson et al.* [2012] (Aug 1998 to Aug 2011)
	−0.62	0.33	−0.46 ± 0.34	*Prinsenberg and Hamilton* [2005] (Aug 1998 to Sep 2001)
Jones Sound	−0.31	0.05		Simulation (1978–2013)
	−0.31	0.03	−0.3	*Melling et al.* [2008] (1998–2002)
Bering Strait	0.88	0.08		Simulation (1978–2013)
			0.8	*Coachman and Aagaard* [1988] (1976–1977)
	0.81	0.27	0.83 ± 0.25	*Roach et al.* [1995] (Sep 1990 to Sep 1994)
	0.86	0.08	0.8	*Woodgate et al.* [2005] (1990–2004)
	0.86	0.08	0.7–1.0	*Woodgate et al.* [2006] (1991–2004)
	0.85	0.08	0.6–1.0	*Woodgate et al.* [2010] (1991–2007)
Barents Sea Opening	2.07	0.36		Simulation (1978–2013)
	2.29	1.39	1.5	*Ingvaldsen et al.* [2004] (Aug 1997 to Aug 2001)
	2.21	0.34	1.8	*Skagseth et al.* [2008] (1997–2006)
Fram Strait	−1.10	0.70		Simulation (1978–2013)
	−0.46	1.03	−4.2 ± 2.3	*Fahrbach et al.* [2001] (Sep 1997 to Sep 1999)
	−0.51	1.12	−2 ± 2 - −4 ± 2	*Schauer et al.* [2004] (Sep 1997 to Aug 2000)
	−0.58	0.50	−2 ± 2.7	*Schauer et al.* [2008] (1997–200s6)
	−0.83	0.74	−1.7	*Rudels et al.* [2008] (1980–2005)

[a]The model-estimated transport was based on the 36 year averaged currents. Note: the positive sign, inflow; the negative sign, outflow.

In Davis Strait, the observed mean volume transports and uncertainties, which were estimated based on combined direct current and hydrographic measurements made over periods of September 1987 to August 1990, October 2004 to September 2005, and October 2004 to September 2010, were −2.6 ± 1.0 Sv [*Cuny et al.*, 2005], −2.3 ± 0.7 Sv [*Curry et al.*, 2011], and −1.6 ± 0.2 Sv [*Curry et al.*, 2014], respectively (Table 1). Since the differences of these three transport values had the same order of magnitude as the measurement uncertainty, we could not estimate the interannual variation of the transport based on these three measurement period data. Correspondingly, the simulated volume transports calculated over the same periods as observations were −1.5, −1.9, and −2.1 Sv (Table 1), which were −1.1 and −0.4 Sv smaller than observed values over the periods of September 1987 to August 1990 and October 2004 to September 2005, respectively, and 0.5 Sv larger than the observed value over the period of October 2004 to September 2010. The simulated volume transport showed a tendency to increase over the three measurement periods. We also estimated the 36 year (1978–2013) averaged volume transport through Davis Strait, which was ∼−1.8 Sv with a standard deviation of ±0.8 Sv (Table 1). This value was very close to the mean value of −2.1 Sv with the uncertainty range of 0.2–1.0 Sv estimated from the measurements of *Cuny et al.* [2005] and *Curry et al.* [2014].

Reasonable agreement between simulated and observed transports in Davis Strait was consistent with the model-data comparisons made in Nares Strait, Lancaster Sound and Jones Sound. Nares Strait is one of the major water passages of Arctic outflow entering the CAA and has a width of ∼35 km. The observed volume transports and uncertainties were −0.67 ± 0.1 Sv [*Sadler*, 1976], −0.8 ± 0.3 Sv [*Münchow et al.*, 2006], −0.91 ± 0.1 Sv [*Münchow et al.*, 2007], and −0.57 ± 0.09 Sv [*Münchow and Melling*, 2008]. These transport values were estimated based on current measurements made across Robeson Channel over the period April–June, 1972, the ship-board ADCP/hydrographic survey data across Kennedy Channel in early August 2003,

four cross-strait ADCP/hydrographic transects taken in August 2003 in Robeson Channel, northern Kennedy Channel, southern Kennedy Channel, and Smith Sound, and 3 year current measurements over the period of August 2003 to August 2006, respectively. The mean transport value averaged over these four measurement periods was −0.74 Sv with the measurement uncertainty range of ±0.09–0.3 Sv.

The AO-FVCOM simulations covered the two measurement periods of August 2003 and August 2003 to August 2006. Correspondingly, the simulated volume transports for these two periods were −0.73 and −0.85 Sv, respectively (Table 1), which were 0.13 Sv smaller than the mean value of −0.86 Sv averaging from *Münchow et al*. [2006] and *Münchow et al*. [2007], and 0.28 Sv larger than the observed value reported by *Münchow and Melling* [2008].

It should be pointed out that the observed transport based on 3 year current measurements over the period of August 2003 to August 2006 [*Münchow and Melling*, 2008] was estimated by excluding the upper 30 m. We recomputed the simulated transport over the same period for the case by excluding the upper 30 m layer, which equaled to −0.68 Sv, 0.17 Sv smaller than the total transport throughout the entire water column. Compared with the observed transport, the simulated transport with excluding the upper 30 m still showed an overestimation by a value of 0.11 Sv. If we considered the measurement uncertainty of 0.09 Sv, the simulated transport was very close to the observed transport. This result also suggested that the uncertainty due to either different sampling resolutions in the vertical and horizontal or model accuracy due to inaccurate external and boundary forcing could be in the range of 0.02 Sv.

The 36 year AO-FVCOM simulation showed that Nares Strait accounted for ∼44% of the total transport through Davis Strait. The simulated 36 year mean transport through Nares Strait was −0.81 Sv with a standard deviation of ±0.33 Sv (Table 1), which was about 0.07 Sv larger than the mean value estimated based on the four measurements. This difference was within the measurement uncertainty range.

Lancaster Sound, located in the west of Baffin Bay, is about 100 km wide. Moored current measurements were initiated in western Lancaster Sound in 1998 and continued until 2011. The observed mean volume transports and standard deviations, estimated based on measurements over the periods of 1988–2001, 1998–2004, and 1998–2006, were -0.75 ± 0.25 Sv [*Prinsenberg and Hamilton*, 2005], -0.7 ± 0.4 Sv [*Melling et al*., 2008], and -0.7 ± 0.3 Sv [*Prinsenberg et al*., 2009], respectively. Using the same measurement data as *Prinsenberg et al*. [2009], *Peterson et al*. [2012] recalculate the mean volume transport over 1998–2006 by introducing an improved algorithm, which produced a transport of −0.53 Sv. It was clear that due to insufficient spatial sampling, the transport estimated by different methods could cause a difference of 0.17 Sv. Using the same approach and extending the data to cover the period of 2007–2011, *Peterson et al*. [2012] reported a mean volume transport and standard deviation of -0.46 ± 0.34 Sv.

Similar to the results shown in *Prinsenberg and Hamilton* [2005], *Melling et al*. [2008], and *Prinsenberg et al*. [2009], the simulated mean transport over the periods with measurements shows minor differences from the 36 year mean value. They were −0.70 Sv over the periods of 1998–2001; −0.68 Sv over the periods of 1998–2004; and −0.65 Sv over the periods of 1998–2006, and −0.62 Sv over the periods of 1998–2011 (Table 1). The simulated transport was 0.12 and 0.16 Sv larger than the values reported by *Peterson et al*. [2012]. These errors were smaller than 0.17 Sv, the difference of transports estimated by *Prinsenberg et al*. [2009] and *Peterson et al*. [2012] with different algorithms. The simulated 36 year mean transport through Lancaster Sound was −0.71 Sv with a standard deviation of ±0.17 Sv and showed that the outflow from Lancaster Sound accounted for ∼39% of the total CAA outflow through Davis Strait.

Jones Sound is located to the north of Lancaster Sound. The two narrow channels, Cardigan Strait and Hell Gate, are water passages in the CAA that outflow through Jones Sound [*Wekerle et al*., 2013]. Several efforts were made to estimate the transport through these two channels and the mean total volume transport estimated based on current measurements over 1988–2002 was −0.3 Sv: −0.2 Sv through Cardigan Strait and −0.1 Sv through Hell Gate [*Melling et al*., 2008]. Correspondingly, over the same period, the simulated mean total transport and a standard deviation through Cardigan Strait and Hell Gate -0.31 ± 0.03 Sv (Table 1), with a difference of 0.01 Sv compared with the observations. The 36 year simulated total transport over the period 1978–2013 through Jones Sound was -0.31 ± 0.05 Sv, implying that the yearly mean transport remained relatively constant, with small interannual variability in the standard deviation range of 0.05 Sv. The 36 year AO-FVCOM simulation showed that the outflow through Jones Sound accounted for ∼17% of the total outflow transport through Davis Strait.

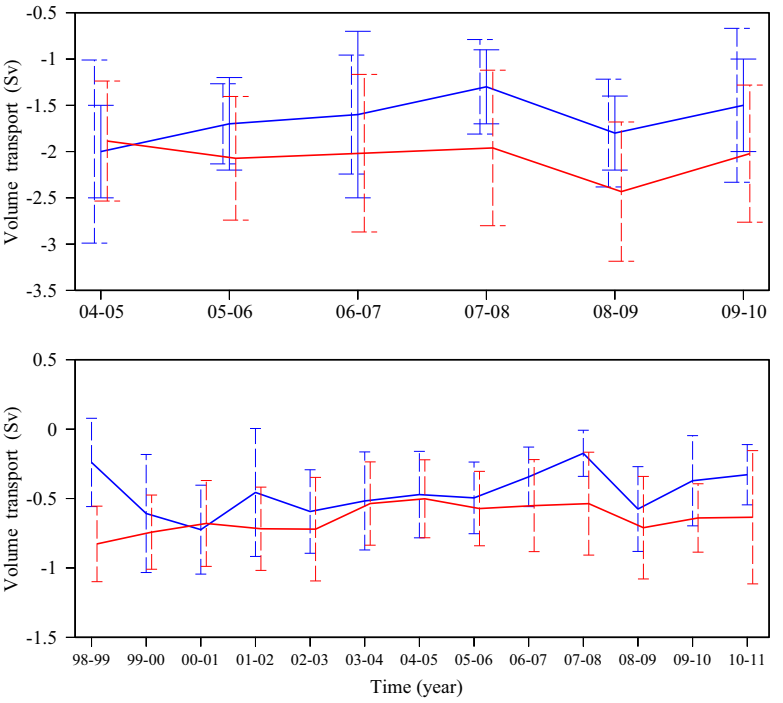

Figure 5. Comparisons of (top) yearly (October–September) simulated (red) and observed (blue) volume fluxes in Davis Strait over the period 2004–2010 and (bottom) yearly (August–July) simulated (red) and observed (blue) volume fluxes in Lancaster Sound over the period 1998–2011. The blue solid vertical bar in the top plot is the observed uncertainty [*Curry et al.*, 2014]. The red and blue dashed vertical bars are the simulated and observed standard deviations.

Several modeling efforts were made to estimate the CAA outflow transport in previous studies. *McGeehan and Maslowski* [2012] used the Naval Postgraduate School Arctic Modeling Effort (NAME) model to simulate the Arctic Ocean circulation over the period 1979–2004. With a horizontal resolution of 1/12° (∼9 km), the simulated 26 year mean volume transport plus standard deviation was −1.55 ± 0.29 Sv through Davis Strait; −0.77 ± 0.17 Sv through Nares Strait, and −0.76 ± 0.12 Sv through Lancaster Sound. The widths of Cardigan Strait and Hell Gate were ∼10 km, which could not be well resolved in NAME, and the transport result from Jones Sound was not described in their paper. The simulated transports were in good agreement with observations in Nares Strait and Lancaster Sound, but about 0.55 Sv lower than the mean observations in Davis Strait. *Wekerle et al.* [2013] applied the unstructured-grid Finite Element Sea ice-Ocean Model (FESOM) to simulate the CAA outflow transport over the period 1968–2007. With a horizontal model resolution of up to ∼5 km, the simulated 40 year mean volume transport was −1.81 ± 0.31 Sv through Davis Strait, −0.91 ± 0.16 Sv through Nares Strait, −0.86 ± 0.16 Sv through Lancaster Sound, and −0.04 ± 0.01 Sv through Jones Strait. The transports estimated by the FESOM and AO-FVCOM had no significant difference in Davis Strait, Nares Strait, and Lancaster Sound, but the FESOM-estimated transport through Jones Sound was ∼0.26 Sv smaller than both the observed and AO-FVCOM values. This difference accounted for 87% of the total transport through this sound.

3.2. Seasonal and Interannual Variability

We compared the AO-FVCOM-simulated annually and monthly averaged volume transports with observations in Davis Strait over the period 2004–2010 summarized by *Curry et al.* [2014] and in Lancaster Sound over the period 1998–2011 described by *Prinsenberg and Hamilton* [2005], *Prinsenberg et al.* [2009], and *Peterson et al.* [2012]. In Davis Strait, the observed annual mean outflow transport was −2.0 Sv over 2004–2005, gradually decreased to −1.3 Sv over 2005–2008, increased to −1.8 Sv over 2008–2009 and then dropped to −1.5 Sv over 2009–2010 (Figure 5, top) [see also *Curry et al.*, 2014]. The simulated annual mean outflow transport was 0.1 Sv smaller over 2004–2005, 0.5, 0.6, and 0.5 larger over 2005–2008, 2008–2009, and 2009–2010, respectively. The measurement uncertainties over these four periods were 0.5, 0.6, 0.4 and 0.5 Sv, respectively. Considering these measurement uncertainties, the simulated annual mean outflow

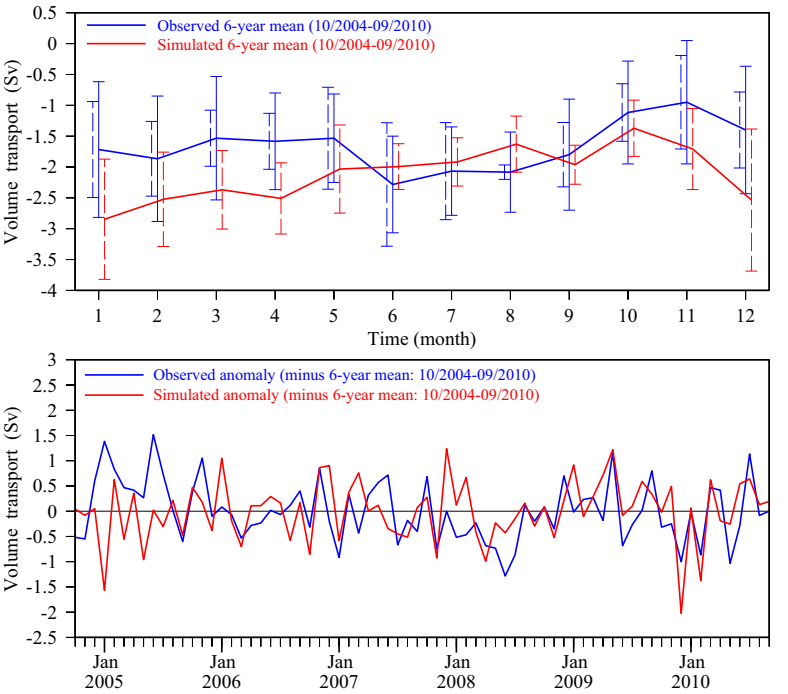

Figure 6. Comparisons of monthly simulated and observed (top) volume fluxes and (bottom) anomalies in Davis Strait over the period 2004–2010. Blue: observed, red: monthly flux and anomaly averaged over the 6 year simulation period of October 2004 to September 2010. The blue solid vertical bar in the top plot is the observational uncertainty. The red and blue dashed vertical bars are the simulated and observed standard deviations.

transport was in reasonable agreement with observations. The AO-FVCOM captured the interannual variability of the outflow through Davis Strait over the measurement periods 2004–2010.

The interannual variability of the outflow transport was also observed and captured by AO-FVCOM in Lancaster Sound (Figure 5, bottom). Both observations and model suggested a decrease over 2002–2008 and an increase over 2008–2009, then a decrease over 2009–2011. Since no measurement uncertainty was given in the observed transport in Lancaster Sound, it was difficult to estimate model errors in this region.

It appeared that the observed and simulated CAA outflow transport through Davis Strait exhibited different seasonal variation patterns (Figure 6, top). Over 2004–2010, the transport estimated by the observed data showed that the 6 year monthly averaged observed transport varied seasonally in a range of ~1.3 Sv, with the minimum value of −1.0 Sv in November and the maximum value of −2.3 Sv in June. The simulated seasonal variability was in a similar range of ~1.4 Sv, but with the minimum value of −1.4 Sv occurring in October and the maximum value of −2.8 Sv occurring in January. Both observed and simulated monthly transport anomalies were in a range of ±1.6 Sv except December 2009, in which the simulated anomaly was above 2.0 Sv (Figure 6, bottom).

The difference between maximum and minimum transports was 1.3 Sv for the observations and 1.4 Sv for the model, which was close to the measurement uncertainty of ~1.1 Sv. For the observations, the transport difference between October and November was only 0.1 Sv, but the measurement uncertainty for these 2 months was 0.8–1.0 Sv. If taking the measurement uncertainty into account, the timing difference between observed and simulated minimum transports should not be significant. Similarly, the observed transport difference between January and June was 0.6 Sv, which was within the measurement uncertainty of 0.8–1.1 Sv. For the same reason, one could not confirm that the transport was larger in June than in January. *Lu et al.* [2014] used the Nucleus for European Modeling of the Ocean (NEMO) to simulate the transport through Davis Strait over the period 1998–2007, and their results also showed a maximum transport in winter rather than summer. It is premature to attribute the difference in the timing of the maximum transport shown in models and observations to the model uncertainty relating to external forcing, ice, and water stratification. There is no doubt, however, that more attention should be paid on this issue in future observations and modeling.

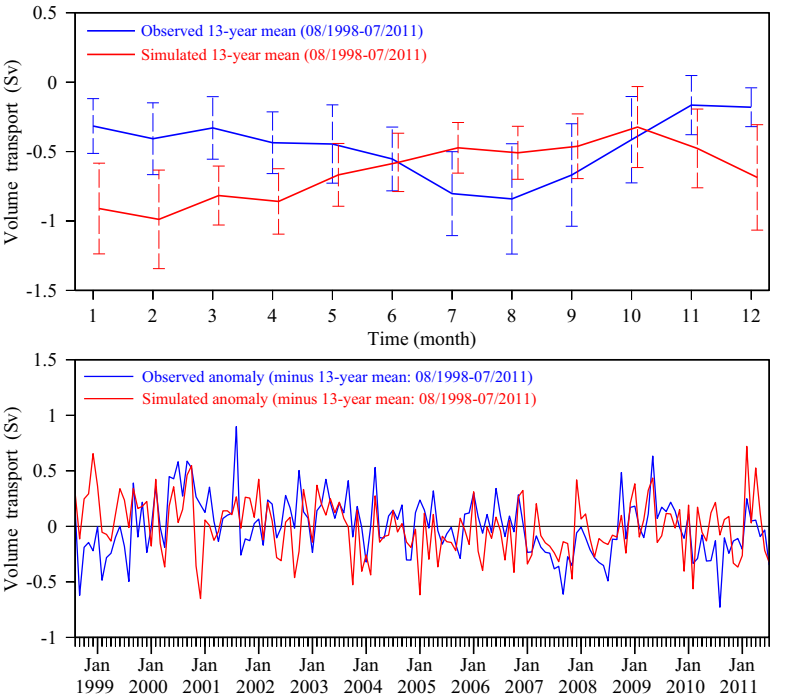

Figure 7. Comparisons of monthly simulated and observed (top) volume fluxes and (bottom) anomalies in Lancaster Sound over the period 1998–2011. Blue: observed, red: monthly flux and anomaly averaged over the 13 year simulation period of August 1998 to July 2011. The red and blue dashed vertical bars in the top plot are the simulated and observed standard deviations.

The AO-FVCOM showed a different pattern in seasonal variability of the outflow flux with the observations through Lancaster Sound (Figure 7). The flux estimated based on current measurements exhibited a minimum in late fall through winter and a maximum in summer [*Prinsenberg and Hamilton*, 2005; *Melling et al*., 2008; *Prinsenberg et al*., 2009]. The simulated minimum flux also occurred in fall, but its maximum flux appeared in winter (Figure 7, top). Except for this disparity, the correlation between simulated and observed interannual anomaly was 0.41 with a critical value of 0.16 at a 95% significance level (Figure 7, bottom). Seasonal variability of the simulated flux was consistent with the NAME [*McGeehan* and *Maslowski*, 2012], which showed a maximum volume flux occurring in March. *McGeehan and Maslowski* [2012] pointed out that the horizontal velocity varied significantly across Lancaster Sound. Since the moorings were mainly placed on the southern shelf where the flow reached the velocity peak in August–September, the flux based on weighted current samplings appeared maxima in summer. We repeated *McGeehan and Maslowski*'s [2012] analysis by calculating the flux with velocities output at the same locations of moorings deployed in Lancester Sound. The flux exhibted a maximum in August if the estimation was made only with currents on the two southern moorings (marked by red triangles) and a maximum in February if the estimation was made only with currents on the two northern moorings (marked by blue triangles). The sum of the flux estimated by currents on these four moorings remained the same seasonal variation pattern as the flux weighted largely on the northern moorings (Figure 8a). Our finding supports *McGeehan and Maslowski*'s [2012] results.

There were no long-term flux data available in Nares Strait for the comparison with the model. According to the time series of the vertically averaged along-strait velocity measured below the 30 m at four mooring across Nares Strait during 2003–2006, the southward flow was strong during January–June, with a peak occurring in the winter [*Münchow and Melling*, 2008]. The AO-FVCOM captured the winter peak of the volume transport through Nares Strait and a coastal-intensified southward flow jet in January–June (Figure 8b).

The AO-FVCOM-estimated fluxes through Davis Strait, Nares Strait, Lancaster Sound and Jones Sound exhibited the same interannual anomaly patterns. With a 99% significance level, the flux correlation was 0.94 between Davis Strait and Nares Strait, 0.97 between Davis Strait and Lancaster Sound, 0.85 between Davis

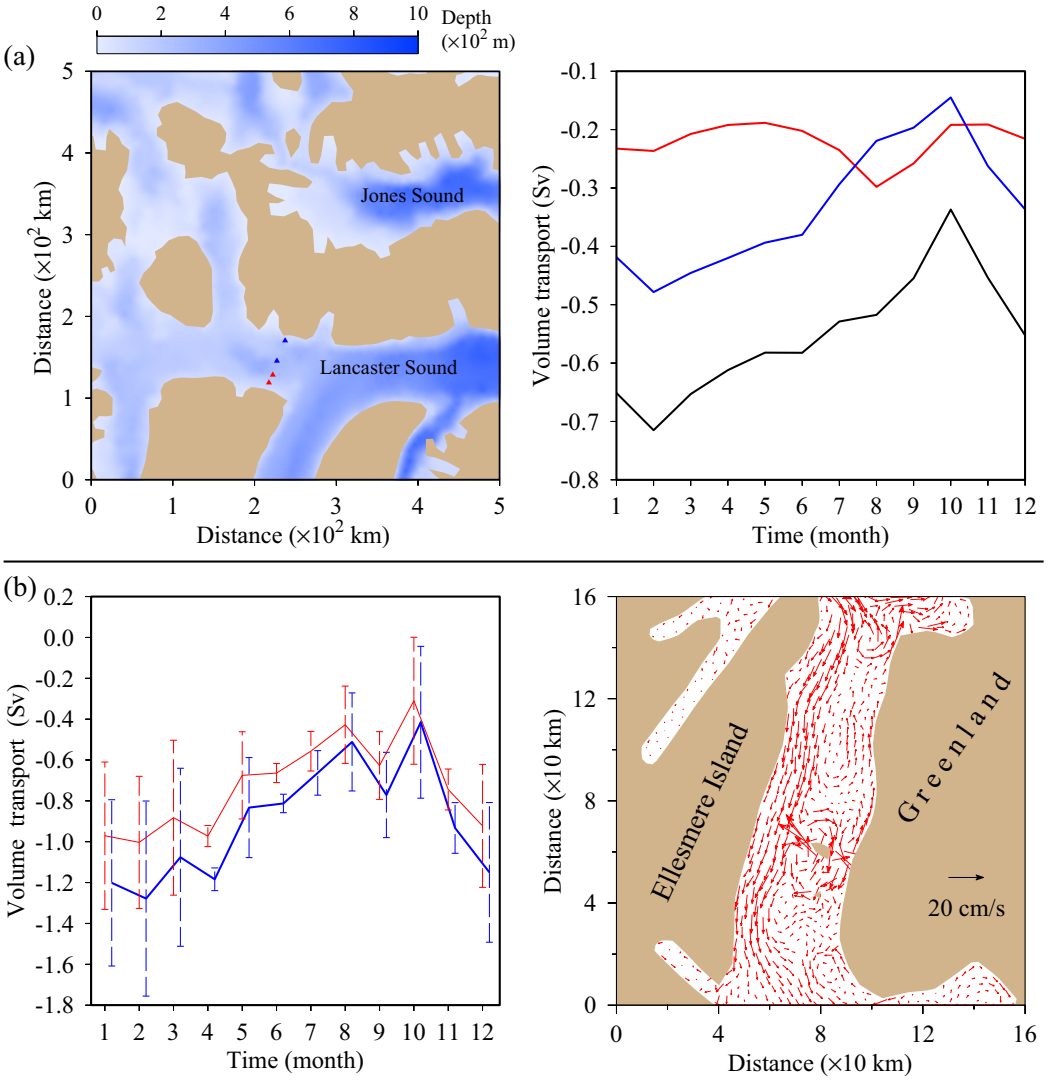

Figure 8. (a) The simulated monthly volume transports (right) through Lancaster Sound were estimated by using the currents at southern shelf moorings (red), northern shelf moorings (blue), and the cross-sound section connected to southern and northern shelf moorings (black) shown in the left plot over the period 1978–2013. (b) The simulated monthly volume transports (left) through Nares Strait for the cases with (blue) and without (red) the inclusion of the upper 30 m over the period 2003–2006. The red vectors are the upper-400 m January–June mean current averaged over the period 2003–2006 in Nares Strait (right).

Strait and Jones Sound and 0.86 between Nares Strait and Lancaster Sound (Figure 9). Our finding was consistent with previous model results in Nares Strait and Lancaster Sound done by NAME over the period 1979–2004 [*McGeehan and Maslowski*, 2012] and by FESOM over the period 1968–2007 [*Wekerle et al.*, 2013]. In Nares Strait, all three models showed similar interannual variability patterns with maxima in 1984 and minima in 1981 and 1988. The FESOM and AO-FVCOM simulations also suggested a minimum flux in 2005. In Lancaster Sound, the three models captured local flux maxima in 1984 and minima in 1981. FESOM simulated a peak in the flux in 1989 [*Wekerle et al.* 2013], which did not appear in NAME. NAME showed a minimum flux in 1988 [*McGeehan and Maslowski*, 2012], which did not appear in FESOM. The flux maxima in 1989 and minima in 1988 were both captured in AO-FVCOM.

4. Dynamics of the CAA Outflow

4.1. Physical Controller of the Arctic-CAA SSH Difference

Previous studies suggested that the volume flux through the major straits in CAA were controlled by the SSH difference between the Arctic Ocean and the downstream exits of the CAA outflow [*Kliem and*

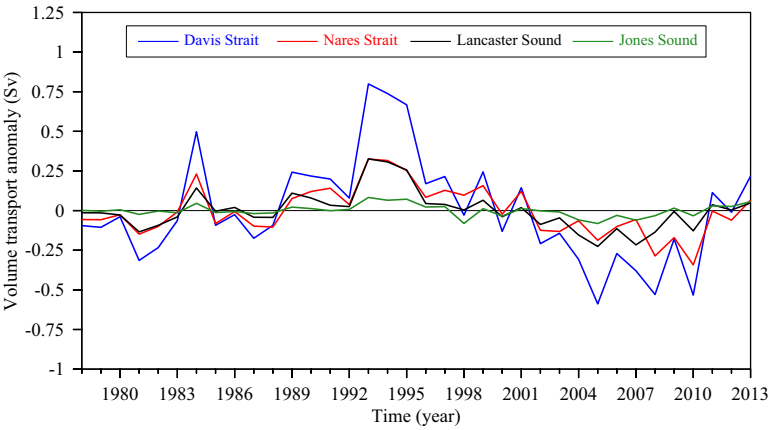

Figure 9. Simulated yearly flux anomalies in Davis Strait (blue), Nares Strait (red), Lancaster Sound (black), and Jones Sound (green) over the period 1978–2013.

Greenberg, 2003; *McGeehan and Maslowski*; 2012; *Wekerle et al*., 2013]. *Kliem and Greenberg* [2003] suggested that a 5 cm increase in the SSH difference between the Arctic Ocean and Baffin Bay could double the volume transport through the CAA. There have been some studies on the mechanisms controlling the SSH

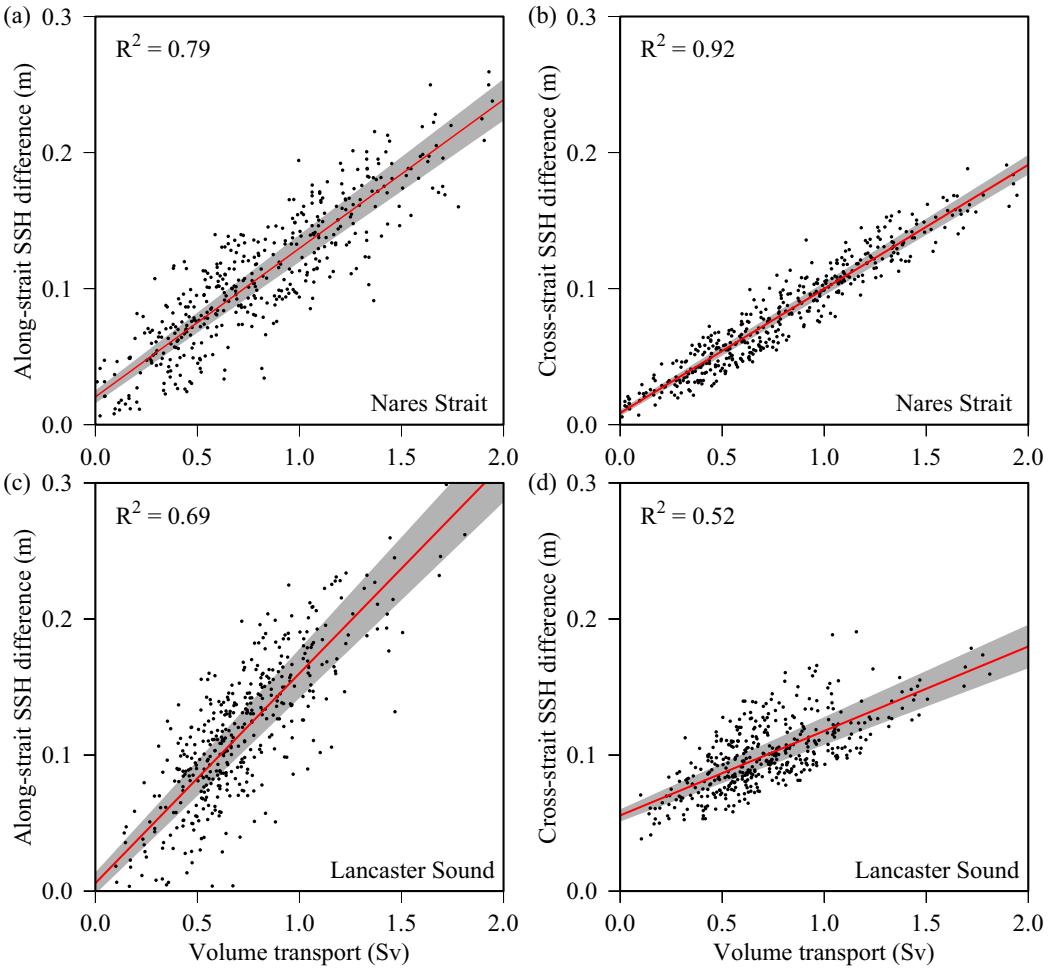

Figure 10. Scatterplots for the monthly volume transports via the along-strait and cross-strait SSH differences and the relations of monthly volume transports through (top) Nares Strait and (bottom) Lancaster Sounds, respectively. Gray shaded area: the 95% confidence bounds of the linear regression fit.

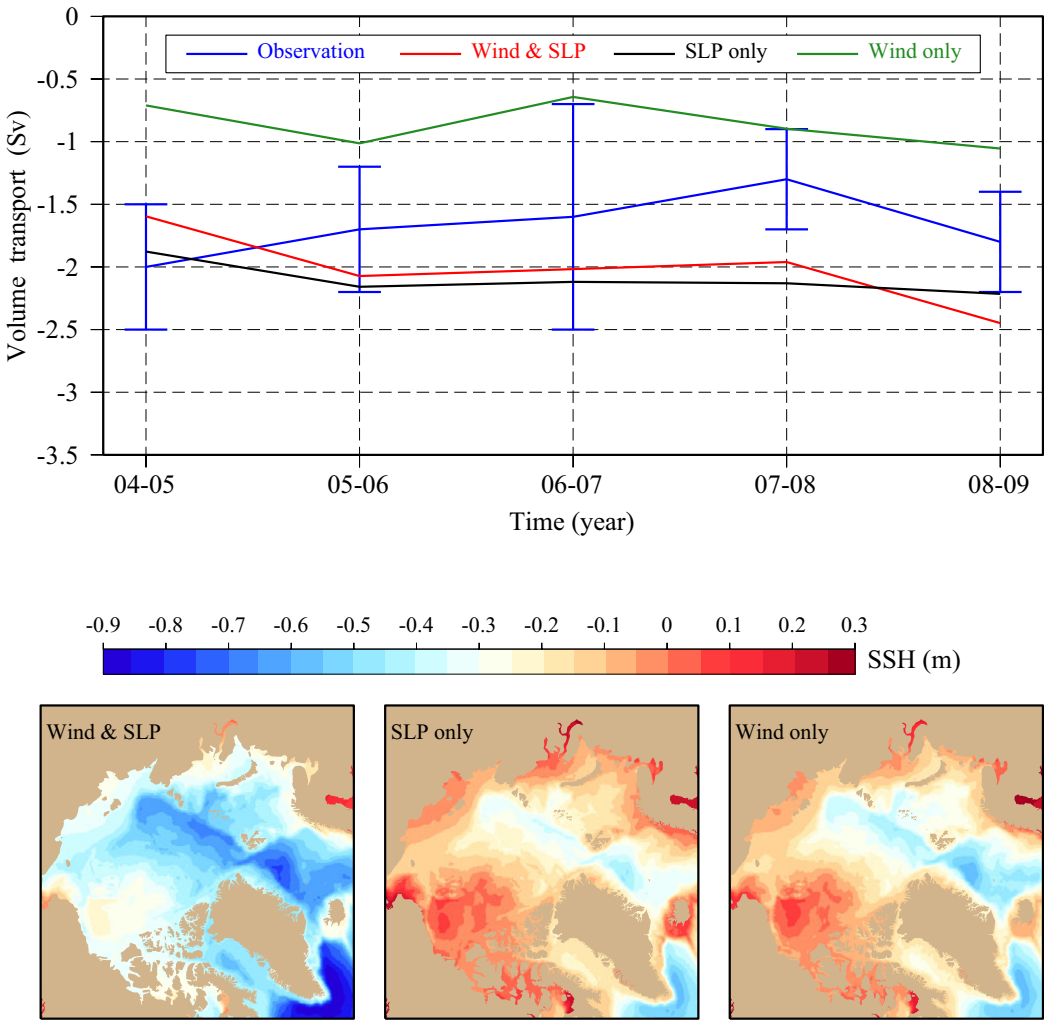

Figure 11. (top) Comparisons of yearly (October–September) observed (blue) and simulated volume fluxes in Davis Strait over the period 2004–2009 for the cases with (1) both wind and SLP forcings (red), (2) only SLP forcing (black), and (3) only wind forcing (green). The blue vertical bar is the observational uncertainty. (bottom) The distributions of the mean SSH field established by the three cases over the period 2004–2009.

difference. *Jahn et al.* [2010] suggested that the basin-scale wind is a dominant forcing to control the CAA outflow. *Houssais and Herbaut* [2011] believed that in the CAA region, the volume transport through Lancaster Sound varied as response to the upstream cross-strait SSH gradient variation driven by the wind stress in the western Arctic, while the transport though Nares Strait is more sensitive to the variability of the downstream SSH in the northern Baffin Bay driven by remote air-sea heat exchange in the Labrador Sea. *McGeehan and Maslowski* [2012] indicated that the wind-induced eddy tended to weaken the northward flow on the western shelf of Greenland (called the West Greenland Current) in Baffin Bay, and the lower temperature and higher salinity in the northeastern Baffin Bay, which was caused by the ice formation, could decrease the SSH in northeastern Baffin Bay and thus enlarge the up-downstream SSH difference in the region. *Wekerle et al.* [2013] obtained a similar conclusion as *Houssais and Herbaut* [2011]. That is, the SSH variation in the downstream of Nares Strait and Lancaster Sound is affected by the air-sea net heat flux in the eastern Baffin Bay and the Labrador Sea. This SSH variation was linked with the North Atlantic Oscillation (NAO). *Lu et al.* [2014] recently reported from their modeling experiments that the SSH difference mechanism varied with seasons and on different locations. The volume transport through Lancaster Sound was not controlled by the wind stress in the upstream region in winter, and the wind in Baffin Bay only had an effect on the SSH variation in spring. In addition, their model results showed no significant correlation of transports through Lancaster Sound and Nares Strait with the air-sea net heat flux.

It should be noticed that many of the previous mechanism studies were conducted with the lack of the relative accurate simulation of the transport observed in the region. The quantitative and reasonable simulation of the CAA outflow obtained by the AO-FVCOM, which is presented in this paper, provided us with a good opportunity to reexamine the SSH-driven mechanism for the CAA outflow. Two questions raised here are: (a) is the AO-FVCOM-simulated CAA outflow correlated with the SSH difference and (b) which physical processes mainly influence the SSH setup and up-downstream difference. To address these questions, we first examined the correlation of the CAA outflow through major straits and sounds with the SSH difference. Then we ran the AO-FVCOM by turning off or on the sea level pressure (SLP) and wind forcing over the period 2004–2009, respectively, during which the model was validated via the observations through Davis Strait. The purpose of doing these two experiments was to assess the relative contribution of SLP and wind forcing to the onset of the SSH difference between the Arctic and Baffin Bay.

The AO-FVCOM 36 year simulation over the period 1978–2013 did show a high correlation between the along-strait sea surface height (SSH) difference with the CAA outflow flux. Examples are given here for the monthly along-strait SSH differences between site-A and site-B in Nares Strait (hereafter referred to as the A-B SSH difference) and between site-C and site-D in Lancaster Sound (hereafter referred to as C-D SSH difference) (Figure 4). We found that the transport-SSH difference correlation was also evident for the cross-strait SSH difference, and examples are given on the section labeled "Sec-N" in Nares Strait, and "Sec-L" in Lancester Sound, respectively (Figure 4). In Nares Strait, the monthly outflow transport was highly correlated with the along-strait SSH difference between site-A and site-B and the cross-strait SSH difference on Sec-N (Figure 10, top), with linear regression correlation coefficients of $R = 0.89$ and $R = 0.96$, respectively. Similarly, in Lancester Sound, the correlations of the monthly outflow transport with either the along-strait SSH difference between site-C and site-D or the cross-strait SSH difference on Sec-L were significantly higher than the critical value of 0.09 at the 95% confidence level, with linear regression correlation coefficients of $R = 0.83$ and $R = 0.72$, respectively (Figure 10, bottom). In both Nares Strait and Lancaster Sound, the outflow transport was proportional to the SSH difference: the higher the SSH difference was, the larger the volume transport was.

Now we examine the key physical mechanism that controlled the SSH difference in the CAA region. For the case with removing the wind forcing (SLP only), the AO-FVCOM-simulated outflow flux through Davis Strait exhibited a similar interannual variation with the case with both wind and SLP (Figure 11, top). The SLP-produced SSH difference between the Arctic and CAA regions was higher over 2004–2008 and lower over 2008–2009, which led the outflow transport to be overestimated by a factor of up to ~4.1–17.6% (0.10–0.28 Sv) and to be underestimated by a factor of up to 9.5% (0.23 Sv), respectively. For the case with removing SLP forcing (wind forcing only), the wind forcing lowered the SSH difference between the Arctic and CAA regions, which caused the outflow transport to be underestimated by a factor of up to 31.9–48.9% (0.89–1.39 Sv) (Figure 11, top). This result demonstrated that the SLP played a critical role in controlling the CAA outflow transport.

In the case of with both SLP and wind forcing, over the period 2004–2009, the mean SSH field in the Arctic Ocean was in the range of −0.9 to −0.1 m, with the values between ~−0.45 and −0.28 m over the Beaufort Sea shelf connecting to the CAA (Figure 11, bottom). Removing either SLP or wind caused the SSH rise in the entire Arctic Ocean, CAA, and adjacent ocean regions, with an value up to 0.3–0.4 m (Figure 11, bottom). Since the reponses of the SSH to either SLP or wind forcing varied in space, the change of the SSH difference between the upstream over the Beaufort Sea shelf and the downstream in Baffin Bay directly contributed to the CAA outflow transport. For the case with SLP only, with a critcal value of 0.23 at a 95% significance level, the correlation between the A-B SSH difference and the outflow transport still remained at a high value of 0.81. Compared with the case with both SLP and wind focing, the A-B SSH difference was 0.8–2.3 cm higher over 2004–2008 and 0.8 m lower over 2008–2009. That was the reason why the outflow transport was slightly overstimated over 2004–2008 and underestimated over 2008–2009 after the wind was removed. For the case with only wind forcing, with the same critical value of 0.23 at a 95% significance level, the correlation between the A-B SSH difference and net flux still remained at a high value of 0.92. However, the A-B SSH difference was 0.5–3.3 cm lower, which led to a significant undersestimation of the outflow transport. If analyzing the 6 year mean values of the SSHs at site-A and site-B, we found that although the SSH over the entire Arctic and CAA regions rised, the rising rate at site-A in the case with SLP only was ~2.3 cm larger than in the case with wind forcing only. Considering the rising rate difference at

Table 2. Comparison Between Velocities and Sea Surface Height Gradients Calculated by the Analytical Solution Derived in Equations (4) and (5) and AO-FVCOM for the Simulation With the CORE-v2 Forcing Over The Period 2004–2009

Year	2004–2005	2005–2006	2006–2007	2007–2008	2008–2009
ρ_1 (kg/m^3)	1025.37	1025.33	1025.34	1025.17	1025.27
ρ_2 (kg/m^3)	1027.41	1027.43	1027.43	1027.41	1027.44
$\bar{\rho}$ (kg/m^3)	1026.39	1026.38	1026.38	1026.29	1026.35
ζ_a (cm)	−39.96	−40.53	−39.73	−40.58	−42.07
ζ_b (cm)	−40.19	−41.43	−40.06	−40.77	−42.37
V_a (cm/s)	2.37	2.13	2.01	2.64	2.20
V_b (cm/s) (Analytical)	21.25	37.00	25.39	19.22	24.15
V_b (cm/s) (AO-FVCOM)	15.28	17.94	17.83	19.08	20.92
$\frac{\partial \zeta_b}{\partial x}$ ($\times 10^{-6}$) (Analytical)	3.12	5.43	3.72	2.82	3.54
$\frac{\partial \zeta_b}{\partial x}$ ($\times 10^{-6}$) (AO-FVCOM)	1.57	1.99	2.01	2.28	2.67

site-B was only 0.6 cm for these two cases, establishing the higher SSH at the CAA entrance over the Beaufort Sea coast by SLP played a major role in controlling the CAA outflow transport.

The variability of the SLP field in the Arctic, CAA, and adjacent oceans is related to both the Arctic Oscillation (AO) and North Atlantic Oscillation (NAO). For this reason, we expect that CAA outflow transport could vary with climate change.

The fact that the outflow transport is highly correlated with both along-strait and cross-strait SSH difference implies that the flow through narrow straits in the CAA was under a simple geostrophic balance in the cross-strait direction. We conducted a scaling analysis of terms in the momentum equations by comparing their magnitudes over the annually averaged scale. In Nares Strait, for example, we found that the flow was dominated in the along-strait direction with the zeroth-order momentum balance between the along-strait advection and along-strait pressure gradient forcing in the along-strait direction and the Coriolis forcing and cross-strait pressure gradient forcing in the cross-strait direction, i.e.:

$$v\frac{\partial v}{\partial y} \sim -\frac{1}{\rho}\frac{\partial P}{\partial y};\ fv \sim \frac{1}{\rho}\frac{\partial P}{\partial x} \tag{1}$$

where x and y are the cross-strait and along-strait axes of the local Cartesian coordinate; v is the along-strait component of the velocity; f is the Coriolis parameter; and P is the pressure. Assuming there is no motion in the lower layer and considering the stratified condition and zeroth-order momentum balance, we could introduce a simple 1.5-layer model to write the above equations in the form of

$$v\frac{\partial v}{\partial y} \sim -g'\frac{\partial h}{\partial y} - \left(g' + \frac{\rho_1}{\bar{\rho}}g\right)\frac{\partial \zeta}{\partial y} \tag{2}$$

$$fv \sim g'\frac{\partial h}{\partial x} + \left(g' + \frac{\rho_1}{\bar{\rho}}g\right)\frac{\partial \zeta}{\partial x} \tag{3}$$

where h is the along-strait component of the thickness of the upper layer; ζ is the sea surface elevation, g' is the reduced gravity defined as $(\rho_2 - \rho_1)g/\bar{\rho}$; and ρ_1 and ρ_2 are the water denisties in the upper and lower layers, respectively. Assuming that h is constant, then equation (2) can be simplied as a typical Bernoulli equation and equation (3) was the geostrophic flow balanced by the Coriolis force and the sea surface elevation gradient. Defining the streamline through site-a and site-b (Figure 4), then the along-strait velocity and cross-strait sea surface elevation gradient at site-b can be determined by

$$v_b \sim \sqrt{2\left(g' + \frac{\rho_1}{\bar{\rho}}g\right)(\zeta_a - \zeta_b) + v_a^2} \tag{4}$$

$$\frac{\partial \zeta_b}{\partial x} \sim \frac{f}{g' + \frac{\rho_1}{\bar{\rho}}g}v_b \tag{5}$$

This solution suggests that in Nares Strait the along-strait velocity in the downstream region is controlled by the sea surface elevation gradient and the cross-strait gradient of the sea surface elevation is proportional to the along-strait velocity. This simple analytical model is consistent with our AO-FVCOM results,

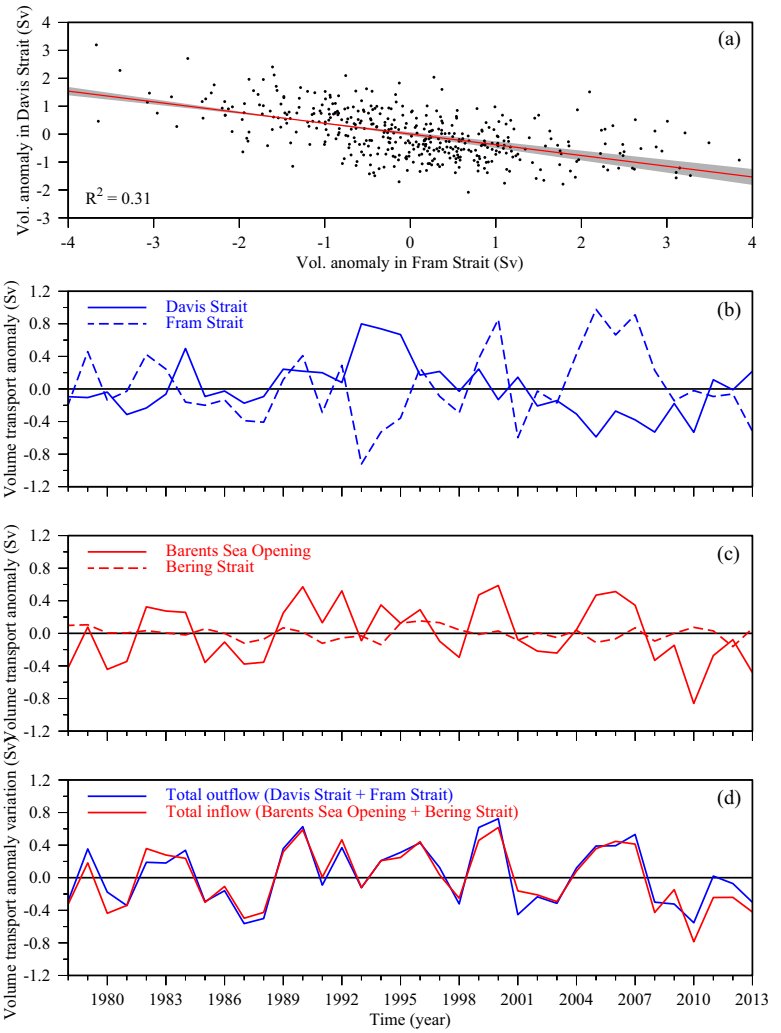

Figure 12. (a) Scatterplot for the monthly volume transports anomalies through Davis Strait and Fram Strait. Red line: the linear regression fit. Gray shaded area: the 95% confidence bound of the fit. (b) Yearly volume transport anomalies through Davis Strait and Fram Strait. (c) Yearly volume transport anomalies through Barents Sea Opening and Bering Strait. (d) Yearly total outflow and inflow transport anomalies.

which showed that the transport in the CAA was highly correlated with the upstream-downstream SSH difference and also with the cross-strait SSH gradient. To check if this mechanism is applicable for the CAA outflow, we calculated the velocity at site-b based on the a-b SSH difference and velocity at site-a on the annually averaged scale over 2004–2009 and found that the velocity calculated by this analytical solution is in the order of magnitude as the velocity output from AO-FVCOM (Table 2). For example, the velocities at site-b calculated by equation (4) over 2007–2008 and 2008–2009 are 19.22 and 24.15 cm/s, respectively, and the AO-FVCOM-computed velocities over these two time periods are 19.08 and 20.92 cm/s, respectively. Similarly, the cross-strait SSH gradient calculated by equation (5) over these two periods are 2.82×10^{-6} and 3.54×10^{-6}, respectively, which are comparable with the AO-FVCOM results of 2.28×10^{-6} and 2.67×10^{-6}.

4.2. Relation of the CAA Outflow With the Net Volume Flux Through Fram Strait

The AO-FVCOM results showed that the change of the CAA outflow transport through Davis Strait affected the net volume flux through Fram Strait. In general, the monthly volume transport anomalies over 1978–2013 through these two straits were negatively correlated, satisfying a linear regression line with a correlation coefficient of −0.56 (Figure 12a). Since the critical value at a 95% significance level was 0.09, the linear correlation was statistically significant. This negative correlation was clearly confirmed in the time series of

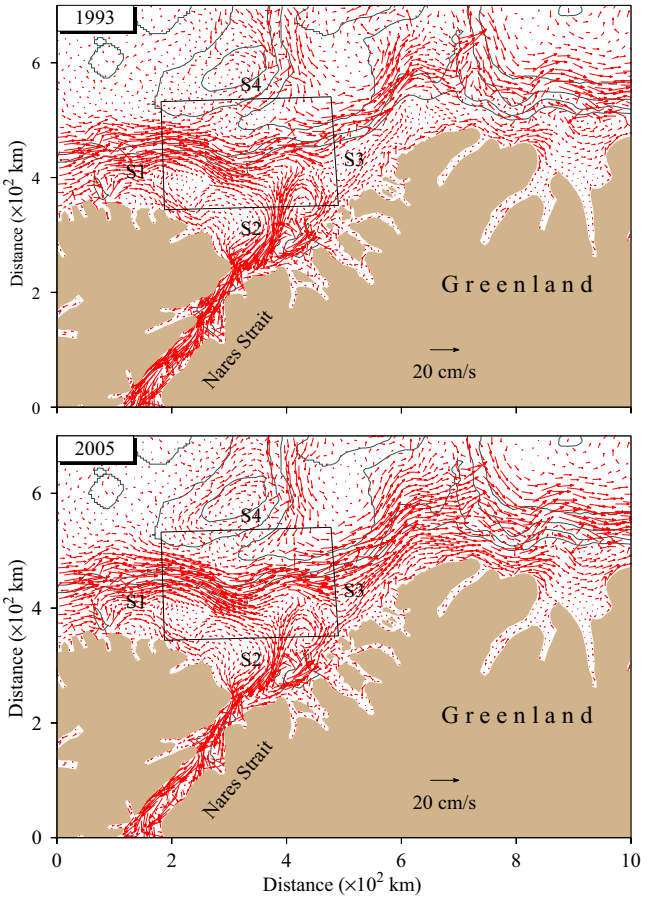

Figure 13. Distributions of the 1993 and 2005 annually mean currents averaged in the upper 400 m over the Beaufort Sea and Greenland shelves connecting to Nares Strait, respectively. Black box: the closed domain used to estimate the volume transport through sections.

yearly volume transport anomalies through Davis and Fram Straits (Figure 12b), particularly during the periods of 1992–1995 and 2003–2008.

The Arctic Ocean consists of inflows from the Pacific Ocean through Bering Strait and from the North Atlantic Ocean through the Barents Sea Opening and the western coast of Spitsbergen of Fram Strait, and outflows through the east Greenland shelf of Fram Strait and the CAA. There were no questions that the net volume flux through Fram Strait could be also affected due to the change of the inflows from those three sources. The AO-FVCOM has provided a reasonable simulation of the inflow transports through Bering Strait and Barents Sea Opening after taking the Norwegian Coastal Current transport at an amount of ~0.6 Sv [*Skagseth et al.*, 2011] into account for the observed inflow transport (Table 1). The annually averaged inflow transport through the Barents Sea Opening varied significantly (up to 0.9 Sv) over the simulation period of 1978–2013, while only a small change (within the range of 0.2 Sv) was found through Bering Strait (Figure 12c). The fluctuation of the inflow from the Barents Sea Opening directly affected the intensity and transport of the cyclonic circulation in the Eurasian Basin and along the Lomonosov Ridge. The outflow along the east Greenland coast of Fram Strait consists of the cyclonic circulation in the Eurasian Basin and the cyclonic slope currents from the Beaufort Sea/Canadian Basin, so that the anomaly of the net volume flux through Fram Strait varied as the Barents Sea inflow and CAA outflow changed. This is clearly evident in Figure 12d, which showed that the model-produced total outflow through Davis Strait and Fram Strait was approximately balanced by the model-produced total inflow from Barents Sea Opening and Bering Strait. Notice that the small unbalanced amount is believed to be due to the uncertainty of the method used in the spatial interpolation when the flux was calculated on selected sections.

The changes of the CAA and Fram Strait outflow transport were closely related to the variation of the slope current over the Beaufort Sea shelf. The years of 1992–1995 and 2003–2008 were the two periods during which the transport anomalies through Fram and Davis Straits were in opposite phases. Years of 1993 and 2005 were selected here as examples to examine how the variation of the slope current affected the CAA and Fram Strait outflow. The 1993 and 2005 annually averaged slope currents over the Beaufort Sea and Greenland shelves exhibited the same pattern, but their spatial distribution and intensity significantly differed (Figure 13). Over the Greenland shelf, the cyclonic slope current was mainly trapped over the shelf break in 1993 but it spread over the entire shelf in 2005. The currents over the shelf connecting to Nares Strait were characterized by the anticyclonic and cyclonic eddy flow fields in both years, but in 2005 a portion of the water left the eastern side of the cyclonic eddy to form the near-coastal current toward the Fram Strait over the Greenland shelf. The existence of this coastal-intensified flow reduced the inflow transport into Nares Strait and in turn increased the outflow transport through Fram Strait. This explained why the net flux through Fram Strait had a negative anomaly in 1993 and a positive anomaly in 2005, with

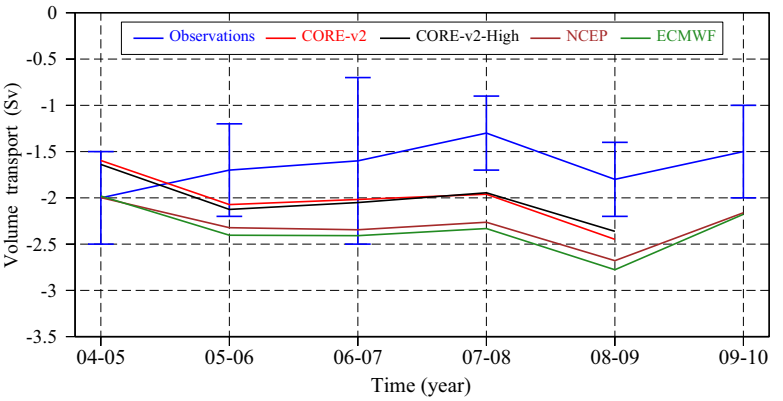

Figure 14. Comparisons between observed and simulated volume fluxes in Davis Strait over the period 2004–2010. Blue: observed; red: CORE-v2; black: CORE-v2 with the refined high-resolution grid in Baffin Bay; brown: NCEP; and green: ECMWF. The blue vertical bar is the observational uncertainty. Note that the CORE-v2 forcing is available until 2009.

corresponding to positive and negative anomalies of the Davis Strait outflow. A closed box shown in Figure 13 was selected to demonstrate the change of the transport into Nares Strait and toward Fram Strait in these two years. Notice that positive and negative signs refer to inflow and outflow, respectively. In 1993 and 2005, the transports through S1, S2, S3, and S4 were 5.70 and 7.34, −1.37 and −0.87, −7.67 and −10.66, and 3.34 and 4.19 Sv, respectively. S2 and S3 are the sections connecting to Nares Strait and toward Fram Strait, respectively. Compared with the transports in 1993, the transports in 2005 through S2 and S3 were 0.50 Sv smaller and 2.99 Sv larger, respectively. S1 is the upstream section, and the larger transport found on this section in 2005 than 1993 was a result of the flow intensification in 2005.

5. Sensitivity Experiment Results

5.1. Model Uncertainties Due to External Forcing and Grid Resolution

In general, the AO-FVCOM produced a relatively larger volume flux through Davis Strait compared with the observations, even though in most years the errors were within the range of the measurement uncertainty (Figure 5). One straightforward thought might be to attribute the differences to the choice of meteorological forcing used to drive the AO-FVCOM and model resolution in Davis Strait. In order to investigate the influence of the atmospheric forcing on the CAA outflow flux, we reran the simulation over the observational periods of 2004–2010 with global NCEP and ECMWF meteorological fields, and compared the flux with results obtained based on CORE-v2 forcing (note the CORE-v2 data set was only updated to 2009). To examine the influence of the model resolution on the CAA outflow flux, we reran the AO-FVCOM with the refined model grid up to ∼8 km in Baffin Bay (see grids in Figure 3).

For a given same model resolution, the flux estimated with three meteorological forcing conditions showed the same trend in interannual variability but different values (Figure 14). The flux estimated with CORE-v2 was closest to the observed flux (except 2004–2005), while the fluxes estimated with ECMWF and NCEP were up to ∼0.4 Sv (15%) larger compared with the CORE-v2 case. The difference between fluxes estimated with ECMWF and NCEP was small, with a maximum value of ∼0.1 Sv. It is clear that the basin-scale surface forcing can increase the model uncertainty in the CAA outflow flux up to 15%.

The AO-FVCOM-simulated A-B and C-D SSH differences in Nares Strait and Lancaster Sound significantly differed for the cases with CORE-v2, NCEP and ECMWF forcings. The larger outflow flux produced in the cases with NCEP and ECMWF forcings cooccurred with the higher SSH difference produced in these two conditions. For example, over the period 2004–2009, in Nares Strait, the A-B SSH difference was about 1.3–1.5 cm higher in the cases with NCEP and ECMWF forcings than in the case with CORE-v2 forcing. Similarly, in Lancaster Sound, the C-D SSH difference was 0.2–0.4 cm higher in the case with NCEP forcing than in the case with CORE-v2 forcing. The C-D SSH difference for the case with ECWMF forcing was 0.7 and 1.1 cm higher in 2007–2008 and 2008–2009.

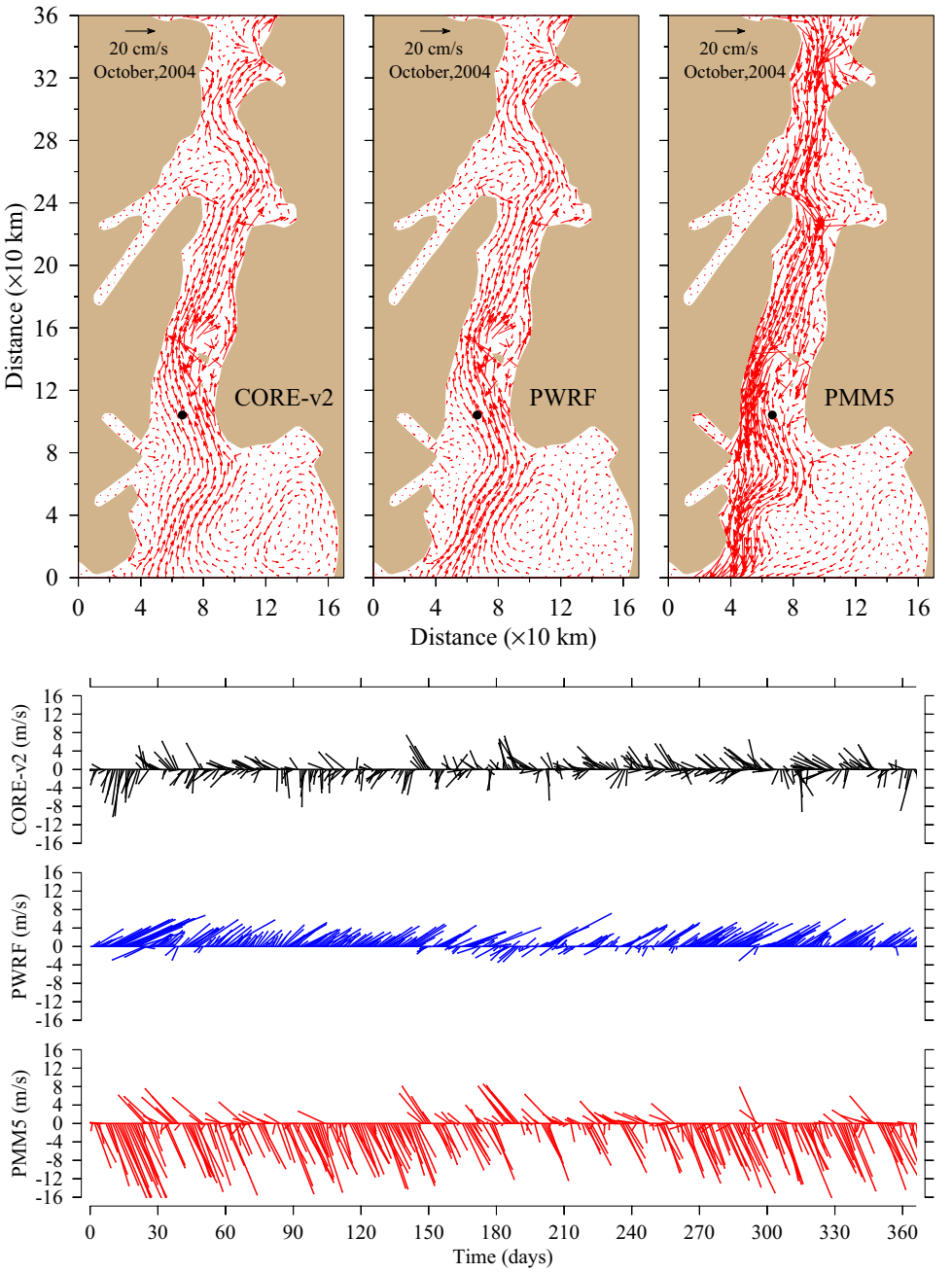

Figure 15. Distributions of the AO-FVCOM-simulated October 2004 monthly mean velocity averaged in the upper 50 m for the cases with (left) CORE-v2, (middle) Polar-WRF, and (right) Polar-MM5. The black dot was the location where the wind vectors for these three meteorological models were compared in bottom plot. Daily wind vectors at the 10 m height over the sea surface in Nares Strait produced by CORE-v2 (black), Polar-WRF (blue), and Polar-MM5 (red) over 2004 (bottom plot).

Although our model results suggested that the SLP is a dominant external forcing controlling the CAA outflow flux, the impact of the wind on the response of the SSH to meteorological forcing and velocity distribution in the CAA region could not be ignored. The fact that winds in the Arctic produced by different meteorological models were so different from each other and that wind measurements were so limited made it difficult to evaluate the wind products. In addition to CORE-v2, NCEP and ECMWF winds, two other wind products are available in the Arctic region. They are (a) the data set of the Arctic System Reanalysis (ASR) Project produced by the 30 km resolution Polar Weather Forecast Model (PWRF) from the Ohio State University [*Byrd Polar Research Center*, 2012] and (b) the data set of the Canadian Archipelago Throughflow Study (CATS) produced by the 6 km

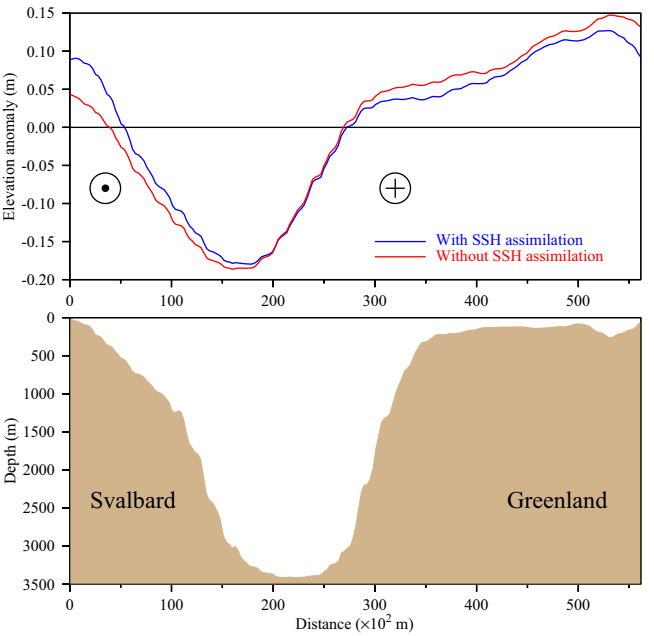

Figure 16. (top) Distributions of the mean SSH anomalies on cross-strait section in Fram Strait for the cases with (blue) and without (red) SSH assimilation over the period 1993–2013. The dot and cross signs with a circle indicate the direction of inflow and outflow through Fram Strait, respectively. (bottom) The cross-strait distribution of the section bathymetry.

resolution Polar MM5 (PMM5) from Oregon State University [*Samelson and Barbour*, 2008]. We directly compared the wind velocity vectors at the 10 m height produced by CORE-v2, PWRF, and PMM5 in Nares Strait, and an example for 2004 is shown in the bottom plot of Figure 15. The high-resolution PMM5-produced wind was mainly southeastward, while the PWRF wind was northeastward dominantly and the CORE-v2 wind varied significanly with time. Correspondingly, the near-surface velocities produced by these three types of wind forcing could differ significantly, particularly in October during which they could flow in an opposite direction (Figure 15, top). The AO-FVCOM produced a western-intensified southward flow in the case with the PMM5-wind, but a northward flow in the cases with CORE-v2 and PWRF. In our 36 year simulation, we did combine the PMM5 wind with the CORE-v2 wind in Nares Strait. *Samelson et al.* [2006] showed evidence that the sea ice drifting through Nares Strait was controlled by the local atmospheric forcing. Since the flow was driven by the ice-sea interfacial stress due to the sea ice drifting in the ice fully covered region, it is clear that we need to implement the high-resolution local wind forcing into the model if we want to improve the near-surface currents in the CAA region.

The horizontal resolution used in the AO-FVCOM 36 year simulation was up to 2 km in the narrow straits in the CAA but was ∼35 km in the interior of Baffin Bay. We reran the simulation over 2004–2009 using the CORE-v2 forcing with the refined horizontal resolution up to ∼8 km in the interior of Baffin Bay. The flux estimated for this refined grid case was only about ∼0.09 Sv or less compared with that for the coarse grid case (Figure 14). In this case, refining the grid in Baffin Bay did not seem to improve the flux estimation through Davis Strait, even though it did improve resolving the flow in the interior of Baffin Bay.

5.2. Change of the Fram Strait Inflow With the SSH Assimilation

The model-data comparison through Fram Strait showed that the model tended to provide a smaller flux than the observations (Table 1). *Chen et al.* [2016] examined the sensitivity of the net flux through Fram Strait to horizontal and vertical sampling resolutions and pointed out that in this inflow-outflow strait, a big bias could be caused due to insufficient samplings. Here we attempt to examine how the net flux could change in the cases with and without the SSH assimilation and also explore the physical reasons that cause the difference. The daily satellite-derived SSH data have been available since 1993. We reran the AO-FVCOM over the period 1993–2013 for the cases with and without the SSH assimilation. The biggest difference found between these two cases was the sea level over both Svalbard and Greenland shelves. This can be seen in the cross-strait distributions of the 1993–2013 mean surface elevation anomalies shown in Figure 16 for these two cases. Over the Svalbard shelf, the surface elevation gradient was ∼10% greater in the case with SSH assimilation than in the case without SSH assimilation. Over the Greenland shelf, the surface elevation gradient produced in the assimilation case was ∼2% smaller. Assuming the flow satisfied a geostrophic balance, the mean barotropic inflow and outflow over the Svalbard and Greenland shelves were ∼10.64 and ∼−6.04 cm/s in the case with SSH assimilation, and ∼9.66 and ∼−6.17 cm/s in the case without SSH assimilation, respectively. The daily adjustment of the model elevation to the satellite-derived SSH in the North Atlantic region outside Fram Strait could produce a larger North Atlantic inflow through

west Svalbard and weaken the outflow from the Arctic Ocean through east Greenland. This explains why the model-simulated net volume flux through Fram Strait was smaller in the case with SSH assimilation.

6. Summary

Davis Strait is the gateway of the CAA outflow originating from the three main passages: Nares Strait, Lancaster Sound, and Jones Sound. This paper is focused on the comparison between the outflow fluxes through Davis Strait simulated by AO-FVCOM and the fluxes estimated from moored measurements and the dominant physical dynamics controlling the CAA outflow flux. The AO-FVCOM used in this study was configured with a high-resolution (up to 2 km) unstructured grid and run with the fully ice-sea coupling dynamics over the period 1978–2013. The model-simulated CAA outflow flux was in reasonable agreement with the flux estimated based on current measurements across Davis Strait, Nares Strait, Lancaster Sound, and Jones Sounds. The model was capable of reproducing the interannual variability of the flux estimated by the current measurements in Davis Strait and Lancaster Sound.

The physical mechanisms that control the variability of the CAA outflow were examined. As the same with previous studies, the AO-FVCOM 36 year simulation over a period 1978–2013 showed a high correlation of the along-strait sea surface height (SSH) difference with the CAA outflow flux. A significant transport-SSH difference correlation was also evident for the cross-strait SSH difference. We have further examined the physical mechanism controlling the SSH difference by running AO-FVCOM for the cases with removal of wind forcing and SLP, respectively. The results show that compared with the wind forcing, SLP played a dominant role in establishing the SSH difference between the upstream Arctic Shelf and downstream Baffin Bay and thus controlling the CAA outflow transport. The correlation of the CAA outflow with the across-strait SSH difference can be explained by a simple geostrophic balance.

The AO-FVCOM results showed that the change of the CAA outflow transport through Davis Strait could affect the net volume flux through Fram Strait. The monthly volume transport anomalies through these two straits were negatively correlated, satisfying a linear regression line with a correlation coefficient higher than the critical value at a 95% significant level. The changes of the CAA and Fram Strait outflow transport were closely related to the variation of the spatial distribution and intensity of the slope currents over the Beaufort Sea and Greenland shelves.

The sensitivities of the model performance to external forcing and grid resolutions were examined by first running AO-FVCOM with three available large-scale atmospheric surface forcing fields (CORE-v2, NCEP, and ECMWF) and two regional-scale surface forcing fields (PMM5 and PWRF) in Nares Strait and second reruning AO-FVCOM with improved grid resolution up to ~8 km in Baffin Bay. The transports obtained from the three large-scale atmospheric forcing cases showed the same trend in interannual variability but different values. The basin-scale surface forcing can increase the model uncertainty in the CAA outflow flux up to 15%. The wind field produced by the high-resolution PMM5 in Nares Strait significantly differed from those produced by the global CORE-v2, ECMWF, and NCEP models as well as the regional PWRF model. Although AO-FVCOM showed that the wind is not a key physical mechanism controlling the CAA outflow flux, the near-surface velocities produced from the cases with the local high-resolution and regional coarse-resoluton meterological models could be in an opposite direction. There is a critical need to improve the meterological forcing in the narrow strait regions of the CAA if one wants to simulate more accurately the near-surface currents in the CAA region. In addition, refining the grid from ~35 to ~8 km in Baffin Bay accounted only for about ~0.09 Sv difference, which was insignificant to the volume flux estimation through Davis Strait.

We also examined the change of the net volume flux through Fram Strait in the cases with and without SSH assimilation. The results showed that the daily adjustment of the model elevation to the satellite-derived SSH in the North Atlantic region outside Fram Strait could produce a larger North Atlantic inflow through west Svalbard and weaken the outflow from the Arctic Ocean through east Greenland.

Acknowledgments

This work was supported by the NSF grants OCE-1203393 for the UMASSD team and PLR-1203643 for Robert C. Beardsley. The Global-FVCOM/AO-FVCOM system was developed with infrastructure support by the Sino-US Joint Innovative Center for Polar Ocean Research (SU-JICPOR), International Center for Marine Studies, Shanghai Ocean University (SHOU). G. Gao was supported by the National Natural Science Foundation of China under the grant 41276197, the Shanghai Pujiang Program under the grant 12PJ1404100, and the Shanghai Shuguang Program. We would like to acknowledge the use of the observational data set collected in Davis Strait provided by Craig Lee (craig@apl.washington.edu) and Beth Curry (beth4cu@uw.edu) and the observational data set collected in Lancaster Sound (ftp://starfish.mar.dfo-mpo.gc.ca/pub/ocean/seaice/Data_Lancaster/Fluxes/). We thank Roger M. Samelson (rsamelson@coas.oregonstate.edu) for providing us the Polar-MM5 atmospheric data. The atmospheric data set of CORE-v2 was obtained from NOAA at http://data1.gfdl.noaa.gov/nomads/forms/core/COREv2/CIAF_v2.html. The reanalysis atmospheric data set of NCEP was generated and distributed by the website of NOAA at ftp://ftp.cdc.noaa.gov/Datasets/ncep.reanalysis/surface_gauss. The data set of ECMWF was available from the website at http://apps.ecmwf.int/datasets/data/interim-full-daily/. The data of Polar-WRF were obtained from NCAR at http://rda.ucar.edu/datasets/ds631.0/. The 36 year simulation was conducted at the SU-JICPOR and we would also like to thank our SHOU collaborators for their efforts on maintenance of the SU-JICPOR cluster for this research.

References

Aagaard, K., and E. Carmack (1989), The role of sea ice and other fresh water in the Arctic circulation, *J. Geophys. Res.*, *94*(C10), 14,485-14,498.

Bleck, R., G. Halliwell, A. Wallcraft, S. Carroll, K. Kelly, and K. Rushing (2002), *HYbrid Coordinate Ocean Model (HYCOM) user's manual: Details of the Numerical Code*, 199 pp., University of Miami, Miami, Fla.

Byrd Polar Research Center, T. O. S. U. (2012), *Arctic System Reanalysis (ASR) Project*, edited, Res. Data Archive at the Natl. Cent. for Atmos. Res., Comput. and Inf. Syst. Lab., Boulder, Colo.

Chassignet, E. P., L. T. Smith, G. R. Halliwell, and R. Bleck (2003), North Atlantic simulations with the Hybrid Coordinate Ocean Model (HYCOM): Impact of the vertical coordinate choice, reference pressure, and thermobaricity, *J. Phys. Oceanogr.*, *33*(12), 2504–2526.

Chassignet, E. P., H. E. Hurlburt, O. M. Smedstad, G. R. Halliwell, P. J. Hogan, A. J. Wallcraft, and R. Bleck (2006), *Ocean prediction with the hybrid coordinate ocean model (HYCOM)*, in Ocean Weather Forecasting, edited by E. Chassignet and J. Verron, pp. 413–426, Springer, Dordrecht, Netherlands.

Chen, C., H. Liu, and R. C. Beardsley (2003), An unstructured, finite-volume, three-dimensional, primitive equation ocean model: Application to coastal ocean and estuaries, *J. Atmos. Oceanic Technol.*, *20*, 159–186.

Chen, C., R. C. Beardsley, and G. Cowles (2006), An unstructured grid, finite-volume coastal ocean model (FVCOM) system, *Oceanography*, *19*, 78–89.

Chen, C., H. Huang, R. C. Beardsley, H. Liu, Q. Xu, and G. Cowles (2007), A finite volume numerical approach for coastal ocean circulation studies: Comparisons with finite difference models, *J. Geophys. Res.*, *112*, C03018, doi:10.1029/2006JC003485.

Chen, C., G. Gao, J. Qi, A. Proshutinsky, R. C. Beardsley, Z. Kowalik, H. Lin, and G. Cowles (2009), A new high-resolution unstructured grid finite volume Arctic Ocean model (AO-FVCOM): An application for tidal studies, *J. Geophys. Res.*, *114*, C08017, doi:10.1029/2008JC004941.

Chen, C., et al. (2013), *An Unstructured-Grid, Finite-Volume Community Ocean Model FVCOM User Manual*, 3rd ed., *Tech. Rep. SMAST/UMASSD-13-0701*, 404 pp., Univ. of Mass. -Dartmouth, New Bedford, Mass.

Chen, C., G. Gao, Y. Zhang, R. C. Beardsley, Z. Lai, J. Qi, and H. Lin (2016), Circulation in the Arcric Ocen: Results from a high-resolution coupled ice-sea nested Global-FVOM and Arctic-FVCOM system, *Prog. Oceanogr.*, *141*, 60–80, doi:10.1016/j.pocean.2015.12.002.

Coachman, L., and K. Aagaard (1988), Transports through Bering Strait: Annual and interannual variability, *J. Geophys. Res.*, *93*(C12), 15,535–15,539.

Cuny, J., P. B. Rhines, and R. Kwok (2005), Davis Strait volume, freshwater and heat fluxes, *Deep Sea Res., Part I*, *52*(3), 519–542.

Curry, B., C. Lee, and B. Petrie (2011), Volume, freshwater, and heat fluxes through Davis Strait, 2004-2005, *J. Phys. Oceanogr.*, *41*(3), 429–436.

Curry, B., C. Lee, B. Petrie, R. Moritz, and R. Kwok (2014), Multiyear volume, liquid freshwater, and sea ice transports through Davis Strait, 2004–2010, *J. Phys. Oceanogr.*, *44*(4), 1244–1266.

Fahrbach, E., J. Meincke, S. Østerhus, G. Rohardt, U. Schauer, V. Tverberg, and J. Verduin (2001), Direct measurements of volume transports through Fram Strait, *Polar Res.*, *20*(2), 217–224.

Galperin, B., L. H. Kantha, S. Hassid, and A. Rosati (1988), A quasiequilibrium turbulent energy model for geophysical flows, *J. Atmos. Sci.*, *45*, 55–62, doi:10.1175/1520-0469(1988)045 < 0055:AQETEM>2.0.CO;2.

Gao, G., C. Chen, J. Qi, and R. C. Beardsley (2011), An unstructured-grid, finite-volume sea ice model: Development, validation, and application, *J. Geophys. Res.*, *116*, C00D04, doi:10.1029/2010JC006688.

Holloway, G., F. Dupont, E. Golubeva, S. Häkkinen, E. Hunke, M. Jin, M. Karcher, F. Kauker, M. Maltrud, and M. Maqueda (2007), Water properties and circulation in Arctic Ocean models, *J. Geophys. Res.*, *112*, C04S03, doi:10.1029/2006JC003642.

Houssais, M. N., and C. Herbaut (2011), Atmospheric forcing on the Canadian Arctic Archipelago freshwater outflow and implications for the Labrador Sea variability, *J. Geophys. Res.*, *116*, C00D02, doi:10.1029/2010JC006323.

Ingvaldsen, R. B., L. Asplin, and H. Loeng (2004), The seasonal cycle in the Atlantic transport to the Barents Sea during the years 1997–2001, *Cont. Shelf Res.*, *24*(9), 1015–1032.

Jahn, A., B. Tremblay, L. A. Mysak, and R. Newton (2010), Effect of the large-scaleatmospheric circulation on the variability of the Arctic Ocean freshwater export, *Clim. Dyn.*, *34*(2-3), 201–222.

Kliem, N., and D. A. Greenberg (2003), Diagnostic simulations of the summer circulation in the Canadian Arctic Archipelago, *Atmos. Ocean*, *41*(4), 273–289.

Lu, Y., S. Higginson, S. Nudds, S. Prinsenberg, and G. Garric (2014), Model simulated volume fluxes through the Canadian Arctic Archipelago and Davis Strait: Linking monthly variations to forcing in different seasons, *J. Geophys. Res. Oceans*, *119*, 1927–1942, doi:10.1002/2013JC009408.

Madec, G., P. Delecluse, M. Imbard, and C. Levy (1998), OPA version 8.1 ocean general circulation model reference manual, *Tech. Rep./Note 11*, 91 pp., LODYC/IPSL, Paris.

Marshall, J., A. Adcroft, C. Hill, L. Perelman, and C. Heisey (1997), A finite-volume, incompressible Navier Stokes model for studies of the ocean on parallel computers, *J. Geophys. Res.*, *102*(C3), 5753–5766.

McGeehan, T., and W. Maslowski (2012), Evaluation and control mechanisms of volume and freshwater export through the Canadian Arctic Archipelago in a high-resolution pan-Arctic ice-ocean model, *J. Geophys. Res.*, *117*, C00D14, doi:10.1029/2011JC007261.

Melling, H., T. A. Agnew, K. K. Falkner, D. A. Greenberg, C. M. Lee, A. Münchow, B. Petrie, S. J. Prinsenberg, R. M. Samelson, and R. A. Woodgate (2008), Fresh-water fluxes via Pacific and Arctic outflows across the Canadian polar shelf, in *Arctic–Subarctic Ocean Fluxes: Defining the Role of the Northern Seas in Climate*, edited by R. R. Dickson, J. Meinke, and P. Rhines, pp. 193–247, Springer, Dordrecht, Netherlands.

Mellor, G. L., and T. Yamada (1982), Development of a turbulence closure model for geophysical fluid problem, *Rev. Geophys.*, *20*(4), 851–875.

Münchow, A., and H. Melling (2008), Ocean current observations from Nares Strait to the west of Greenland: Interannual to tidal variability and forcing, *J. Mar. Res.*, *66*(6), 801–833.

Münchow, A., H. Melling, and K. K. Falkner (2006), An observational estimate of volume and freshwater flux leaving the Arctic Ocean through Nares Strait, *J. Phys. Oceanogr.*, *36*(11), 2025–2041.

Münchow, A., K. K. Falkner, and H. Melling (2007), Spatial continuity of measured seawater and tracer fluxes through Nares Strait, a dynamically wide channel bordering the Canadian Archipelago, *J. Mar. Res.*, *65*(6), 759–788.

Pacanowsky, R., and S. Griffies (1999), *The MOM3 Manual*, 680 pp., Geophys. Fluid Dyn. Lab./NOAA, Princeton, N. J.

Peterson, I., J. Hamilton, S. Prinsenberg, and R. Pettipas (2012), Wind-forcing of volume transport through Lancaster Sound, *J. Geophys. Res.*, *117*, C11018, doi:10.1029/2012JC008140.

Price, J., R. Weller, and R. Pinkel (1986), Diurnal cycling: Observations and models of the upper-ocean response to diurnal heating, cooling, and wind mixing, *J. Geophys. Res.*, *91*(C7), 8411–8427.

Prinsenberg, S., and J. Hamilton (2005), Monitoring the volume, freshwater and heat fluxes passing through Lancaster Sound in the Canadian Arctic Archipelago, *Atmos. Ocean*, *43*(1), 1–22.

Prinsenberg, S., J. Hamilton, I. Peterson, and R. Pettipas (2009), Observing and interpreting the seasonal variability of the oceanographic fluxes passing through Lancaster Sound of the Canadian Arctic Archipelago, in *Influence of Climate Change on the Changing Arctic and Sub-Arctic Conditions*, edited by J. Nihoul and A. Kostianoy, pp. 125–143, Springer, Dordrecht, Netherlands.

Proshutinsky, A., M. Steele, J. Zhang, G. Holloway, N. Steiner, S. Hakkinen, D. Holland, R. Gerdes, C. Koeberle, and M. Karcher (2001), Multinational effort studies differences among Arctic Ocean models, *Eos Trans. AGU*, *82*(51), 637–644.

Roach, A., K. Aagaard, C. Pease, S. Salo, T. Weingartner, V. Pavlov, and M. Kulakov (1995), Direct measurements of transport and water properties through the Bering Strait, *J. Geophys. Res.*, *100*(C9), 18,443–18,457.

Rudels, B., M. Marnela, and P. Eriksson (2008), Constraints on estimating mass, heat and freshwater transports in the Arctic Ocean: An exercise, in *Arctic–Subarctic Ocean Fluxes: Defining the Role of the Northern Seas in Climate*, edited by R. R. Dickson, J. Meincke, and P. Rhines, pp. 315–341, Springer, Dordrecht, Netherlands.

Sadler, H. E. (1976), Water, heat, and salt transports through Nares Strait, Ellesmere Island, *J. Fish. Board Can.*, *33*(10), 2286–2295.

Samelson, R., and P. Barbour (2008), Low-level jets, orographic effects, and extreme events in Nares Strait: A model-based mesoscale climatology, *Mon. Weather Rev.*, *136*(12), 4746–4759.

Samelson, R. M., T. Agnew, H. Melling, and A. Münchow (2006), Evidence for atmospheric control of sea-ice motion through Nares Strait, *Geophys. Res. Lett.*, *33*, L02506, doi:10.1029/2005GL025016.

Schauer, U., E. Fahrbach, S. Osterhus, and G. Rohardt (2004), Arctic warming through the Fram Strait: Oceanic heat transport from 3 years of measurements, *J. Geophys. Res.*, *109*, C06026, doi:10.1029/2003JC001823.

Schauer, U., A. Beszczynska-Möller, W. Walczowski, E. Fahrbach, J. Piechura, and E. Hansen (2008), Variation of measured heat flow through the Fram Strait between 1997 and 2006, in *Arctic–Subarctic Ocean Fluxes: Defining the Role of the Northern Seas in Climate*, , edited by R. R. Dickson, J. Meinke, and P. Rhines, pp. 65–85, Springer, Dordrecht, Netherlands.

Schlichtholz, P., and M.-N. Houssais (1999), An inverse modeling study in Fram Strait. Part I: Dynamics and circulation, *Deep Sea Res., Part II*, *46*(6), 1083–1135.

Skagseth, Ø., T. Furevik, R. Ingvaldsen, H. Loeng, K. A. Mork, K. A. Orvik, and V. Ozhigin (2008), Volume and heat transports to the Arctic Ocean via the Norwegian and Barents Seas, in *Arctic–Subarctic Ocean Fluxes: Defining the Role of the Northern Seas in Climate*, edited by R. R. Dickson, J. Meinke, and P. Rhines, pp. 45–64, Springer, Dordrecht, Netherlands.

Skagseth, Ø., K. F. Drinkwater, and E. Terrile (2011), Wind- and buoyancy-induced transport of the Norwegian Coastal Current in the Barents Sea, *J. Geophys. Res.*, *116*, C08007, doi:10.1029/2011JC006996.

Smagorinsky, J. (1963), General circulation experiments with the primitive equations, I. The basic experiment, *Mon. Weather Rev.*, *91*, 99–164.

Smith, R., and P. Gent (2002), Reference manual for the Parallel Ocean Program (POP), ocean component of the Community Climate System Model (CCSM2. 0 and 3.0), *Tech. Rep. LA-UR-02-2484*, Los Alamos Natl. Lab., Los Alamos, N. M.

Steele, M., R. Morley, and W. Ermold (2001), PHC: A global ocean hydrography with a high quality Arctic Ocean, *J. Clim.*, *14*, 2079–2087, doi:10.1175/1520-0442(2001)014 < 2079:PAGOHW>2.0.CO;2.

Straneo, F., and F. J. Saucier (2008), The Arctic–Subarctic exchange through Hudson Strait, in *Arctic–Subarctic Ocean Fluxes: Defining the Role of the Northern Seas in Climate*, edited by R. R. Dickson, J. Meinke, and P. Rhines, pp. 249–261, Springer, Dordrecht, Netherlands.

Tang, C. C., C. K. Ross, T. Yao, B. Petrie, B. M. DeTracey, and E. Dunlap (2004), The circulation, water masses and sea-ice of Baffin Bay, *Prog. Oceanogr.*, *63*(4), 183–228.

Wekerle, C., Q. Wang, S. Danilov, T. Jung, and J. Schröter (2013), The Canadian Arctic Archipelago throughflow in a multiresolution global model: Model assessment and the driving mechanism of interannual variability, *J. Geophys. Res. Oceans*, *118*, 4525–4541, doi:10.1002/jgrc.20330.

Woodgate, R. A., E. Fahrbach, and G. Rohardt (1999), Structure and transports of the East Greenland Current at 75 N from moored current meters, *J. Geophys. Res.*, *104*(C8), 18,059–18,072.

Woodgate, R. A., K. Aagaard, and T. J. Weingartner (2005), Monthly temperature, salinity, and transport variability of the Bering Strait through flow, *Geophys. Res. Lett.*, *32*, L04601, doi:10.1029/2004GL021880.

Woodgate, R. A., K. Aagaard, and T. J. Weingartner (2006), Interannual changes in the Bering Strait fluxes of volume, heat and freshwater between 1991 and 2004, *Geophys. Res. Lett.*, *33*, L15609, doi:10.1029/2006GL026931.

Woodgate, R. A., T. Weingartner, and R. Lindsay (2010), The 2007 Bering Strait oceanic heat flux and anomalous Arctic sea-ice retreat, *Geophys. Res. Lett.*, *37*, L01602, doi:10.1029/2009GL041621.